# 31 Neutron-Induced Prompt Gamma Activation Analysis (PGAA)

*Z. Révay*[1] · *R. M. Lindstrom*[2] · *E. A. Mackey*[2] · *T. Belgya*[1]
[1]Hungarian Academy of Sciences, Budapest, Hungary
[2]National Institute of Standards and Technology, Gaithersburg, MD, USA



Attila Vértes, Sándor Nagy, Zoltán Klencsár, Rezső G. Lovas & Frank Rösch (eds.), *Handbook of Nuclear Chemistry*,
DOI 10.1007/978-1-4419-0720-2_31, 

**Abstract:** This section presents the principles, the practical aspects, and the applications of neutron-induced prompt gamma activation analysis (PGAA). The fundamentals of the method, the characteristics of the analytical technique, and the instrumentation are introduced. The measurements of samples and standards together with the procedures of the quantitative analysis are described. High-energy gamma-ray spectroscopy, enabling reliable chemical analyses, is discussed in detail. A comprehensive section of the most recent applications of the PGAA method is also given.

## 31.1 Introduction

While investigating the capture reaction of neutrons in hydrogenous materials, the emission of a highly penetrating gamma radiation had already been observed in 1934 (Lea 1934). This was the first prompt gamma radiation ever detected. Now it is known as the prompt gamma ray of 2,223.2487 keV energy from the reaction $H(n,\gamma)^2H$.

Whenever a nucleus absorbs a neutron, its binding energy is released in the form of the so-called prompt gamma radiation. If the product nuclide is stable, the process ends here. If it is radioactive, then it decays away while emitting typically a beta particle, mostly followed by gamma rays, too. Both types of gamma radiation are characteristic of the capturing nucleus, and thus are suitable for elemental analysis. Neutron activation analysis is based on the detection of the decay-gamma radiation (see Chap. 30 in this Volume), while prompt gamma activation analysis (PGAA) utilizes both, but mainly the prompt radiation.

Both activation analytical techniques require powerful neutron sources. The first reactor-based PGAA measurement was performed by Isenhour and Morrison in 1966 (1966a, b) using a chopped neutron beam from a reactor and detecting the gamma rays with a NaI(Tl) detector. In the late 1960s, a major breakthrough was the introduction of semiconductor detectors, whose energy resolution was more than an order of magnitude better than that of the best scintillators. The performance of the PGAA technique has further increased thanks to the new Ge(Li)–NaI(Tl) Compton-suppressed systems (Orphan and Rasmussen 1967). Neutron guides at research reactors were also introduced to this analytical method: first at the Saclay reactor in 1969 (Comar et al. 1969a, b), and then at the high-flux reactor in Grenoble (Henkelmann and Born 1973), while several facilities have been established at collimated reactor beams (Molnár 2004). The application of the PGAA method has increased thanks to the availability of high-flux thermal and cold beams during the 1990s at National Institute of Standards and Technology (NIST), USA (Lindstrom et al. 1993), at Jülich Research Center, Germany (Rossbach 1991), at Japanese Atomic Energy Research Center (JAERI), Japan (Yonezawa et al. 1993) and at the Budapest Neutron Center, Hungary (Molnár et al. 1997). Several other systems have been put into operation since then.

One of the reasons that PGAA was held back from common use was the lack of a proper analytical database. The first systematic series of measurements of capture-gamma spectra for 75 elements was performed by a group at Massachusetts Institute of Technology (MIT) at the end of the 1960s (Orphan et al. 1970; Rasmussen et al. 1969). The best-known compilation of these data was published by Lone et al. (1981). The "Lone table" and its electronic version have been the only source of spectroscopic data for scientists working in the field of PGAA for more than 20 years. The first complete catalog of prompt gamma lines appeared only in 2004 based on the measurements at the Budapest Research Reactor by Révay et al. (Molnár 2004).

## 31.2 Fundamentals of Prompt Gamma Activation Analysis

### 31.2.1 Fundamental Processes

Neutrons are elastically or inelastically scattered, or absorbed when they interact with matter. The most essential reaction induced by neutrons in matter is *radiative neutron capture*, or the **(n,γ) reaction** (see Chap. 30 in this Volume). Prompt gamma radiation is emitted by the excited nuclei after the capture, releasing the binding energy of the neutron (typically 6–9 MeV) within $10^{-14}$ s. If radioactive isotopes are produced, delayed gamma radiation can also be detected with energies up to 2–3 MeV. Decay gamma radiation from short-lived nuclides can also be observed in prompt gamma measurements.

Other important competing reactions that can occur in samples, are the neutron-induced emission of charged particles, specifically (n,p), (n,α) reactions, and fission, noted as (n,f) reaction (Molnár 2004). The most important cases are the following:

- (n,p) reactions on: $^{3}$He and $^{14}$N
- (n,α) reactions on: $^{6}$Li and $^{10}$B
- (n,f) reaction on: $^{235}$U

Light nuclides have weak (n,γ) branching, while their charged-particle emission branch is much stronger. In the case of $^{10}$B, the emission of the alpha particle is followed by the emission of a gamma ray from the residual $^{7}$Li nucleus with the energy of 478 keV. Because of the recoil of the nucleus, the spectrum peak is characteristically broadened over an energy range of about 15 keV. This strong peak makes possible the unambiguous identification of *boron*.

In the case of fissile nuclides, fission can be the dominant reaction. From among the naturally occurring nuclides, it is $^{235}$U whose fission cross section is significant— 583 barn— while the capture cross section is 98 barn. During fission, energy of about 15 MeV is released in the form of gamma radiation, which is more than in the case of neutron capture, for which the binding energy is 6.395 MeV. This action results in a characteristic shape of the spectrum with a much steeper low-energy trend, compared to a spectrum from (n,γ) reactions only.

For bulk samples, elastic scattering of the neutrons before the capture reaction may also play an important role, lengthening the path of the neutrons inside the target. The energy distribution of the neutrons may also be modified by elastic scattering especially in the case of hydrogenous materials.

The neutron-capture cross section of the (n,γ), (n,p), and (n,α) reactions typically follow the **1/*v* law** for low neutron energy. For these *regular nuclides,* the cross section can be described using the following expressions:

$$\sigma(v) = \sigma_0 \frac{v_0}{v} \qquad \sigma(E) = \sigma_0 \sqrt{\frac{E_0}{E}} \qquad \sigma(\lambda) = \sigma_0 \frac{\lambda}{\lambda_0} \tag{31.1}$$

where $\sigma_0$ is the thermal cross section, $v_0 = 2{,}200$ m s$^{-1}$, $E_0 = 25.26$ meV, $\lambda_0 = 1.80$ Å. In the cold energy range (below 10 meV) all nuclides are regular. The $1/v$ dependence continues until the first resonance (if any). Most resonances appear in the eV – keV neutron kinetic energy range. In some cases, the lowest energy resonances partly overlap with the thermal region ($^{113}$Cd, $^{149}$Sm, etc.), resulting in an increase of the capture cross section. These *irregular nuclides* will have an increased reaction rate in thermal beams relative to the regular ones. This discrepancy can be corrected with the so-called Westcott *g* factor (Westcott 1955).

### 31.2.2 Activation Equations

In PGAA, one is interested in the correlation of the characteristic spectral peak areas and the masses of the emitting components. The calculation here is simpler, for many reasons, than in neutron activation analysis (NAA):

- In PGAA, the activation takes place in an almost parallel beam instead of an isotropic neutron field. Thus, the attenuation of neutrons can be calculated in a simpler way.
- The spectrum peaks from prompt gamma radiation are acquired only during the activation; hence, peak areas do not need to be corrected for decay.
- Many neutron beams contain only a small amount of epithermal and fast neutrons, and thus any reaction induced by them can normally be neglected.

The simplest equation for the reaction rate produced by a parallel beam of monochromatic neutrons in an ideally thin and homogeneous sample can be written as follows:

$$R = n\,\sigma\,\Phi \tag{31.2}$$

where $R$ is the reaction rate ($s^{-1}$), $n$ is the number of atoms of the examined nuclide in the neutron beam, $\sigma$ is the cross section for neutron capture at the given energy ($cm^2$), and $\Phi$ is the neutron flux ($cm^{-2}\,s^{-1}$). For the characterization of a given gamma ray, the so-called partial gamma-ray production cross section is used:

$$\sigma_\gamma = \theta\,\sigma\,P_\gamma \tag{31.3}$$

where $\theta$ is the natural abundance of the given isotope in the element of interest, $\sigma$ is the isotopic capture cross section, and $P_\gamma$ is the emission probability of the gamma ray with the given energy and gives the fraction of the emitted gamma photons per capture. The count rate of a peak at a given energy in the gamma spectrum can be written as

$$\rho_\gamma = \varepsilon(E_\gamma)\,n\,\sigma_\gamma\,\Phi = \varepsilon(E_\gamma)\,\frac{m}{M}\,N_A\,\sigma_\gamma\,\Phi \tag{31.4}$$

where $\rho_\gamma$ is the count rate, i.e., the net peak area divided by the measuring time (live time of the counting system) and $\varepsilon(E_\gamma)$ is the counting efficiency of the detector (see later), $m$ is the mass of the element, $M$ is its atomic weight, and $N_A$ is the Avogadro constant.

In many practical cases, the neutrons follow an energy distribution, the cross section is energy-dependent, the sample may not be regarded as ideally thin, and thus the modification of the neutron field and the attenuation of gamma rays within the sample must also be taken into account. Instead of considering all these effects, simplifying assumptions may be introduced. Let us examine two limiting cases in more detail, which can be approximated in reality quite well (Molnár 2004).

#### 31.2.2.1 Thin Sample Approximation

When irradiating a homogeneous and thin sample, the gamma-ray self-absorption, neutron self-shielding, as well as other effects, modifying the counting efficiency and the variation of the internal flux inside the sample can be neglected. Thus the reaction rate, as shown in

Chap. 30 in Vol. 3, depends on the integral of the product of the partial cross section and the neutron flux. For a regular nuclide (i.e., whose cross section follows the $1/v$ law), this integral can be replaced with the product of two average quantities:

$$\int_0^\infty \sigma_\gamma(E_n)\Phi(E_n)\,dE_n = \sigma_{\gamma 0}\Phi_0 \tag{31.5}$$

where $\sigma_{\gamma 0}$ is the partial gamma-ray production cross section measured with monochromatic neutrons having the speed of $v_0 = 2{,}200$ m s$^{-1}$, which equals the cross section determined in a neutron beam having a thermal distribution with the temperature of 293 K, and $\Phi_0$ (sometimes written as $\Phi_{th}$) is the *thermal equivalent neutron flux*:

$$\Phi_0 = \frac{v_0}{\langle v \rangle}\Phi_r \tag{31.6}$$

where $\Phi_r$ is the real flux, i.e., the actual number of neutrons reaching a unit surface of the sample in a second. When activating in a cold neutron beam, the reaction rate becomes higher due to the increase of the cross section, which is inversely proportional to the average speed. In PGAA, however, the use of thermal cross sections is preferred for their conceptual simplicity. The speed dependence is taken into account by using the thermal equivalent flux, which is inversely proportional to the average speed. (As can be seen from Eq. (31.1), it is also inversely proportional to the square root of the average energy and is proportional to the average wavelength.) Using $\Phi_0$, the reaction rate expressions become similar to Eqs. (31.2) and (31.4):

$$R^0 = n\sigma_0\Phi_0 \qquad \rho_\gamma^0 = \frac{m}{M}N_A\,\sigma_{\gamma 0}\,\Phi_0\,\varepsilon(E_\gamma) \tag{31.7}$$

It should be mentioned that in this approximation, the count rate depends only on the mass of the component in the beam, and it does not depend on the sample shape, or even the surface area facing the beam (Molnár 2004).

### 31.2.2.2 "Black" Sample Approximation

In the other limiting case, one of the major components has an extremely large capture cross section, so all the neutrons are absorbed close to the surface in the sample, and every neutron generates gamma photons according to the emission probabilities of the capturing nuclide. The observed count rate does not depend on the cross section any more, but it is directly proportional to the number of neutrons, i.e., the real flux multiplied by the emission probability:

$$\rho_\gamma^\infty = S\,P_\gamma\,\Phi_r\,\varepsilon(E_\gamma) \tag{31.8}$$

where $S$ is the surface area of the sample facing the beam, $P_\gamma$ is the emission probability, and $\Phi_r$ is the real flux. If the real flux of two different beams is the same, the count rate for black samples will be the same, too. Using black samples, the real flux becomes a directly measurable quantity. Comparing it with the thermal equivalent flux based on Eqs. (31.6) and (31.7) the average speed or wavelength of the beam can be determined (Molnár 2004; Révay 2005).

## 31.3 Characteristics of PGAA

### 31.3.1 Analytical Properties

The most important characteristic of PGAA is based on the fact that both the neutrons and the emitted gamma radiation are highly penetrating. For example, an iron plate with a thickness of 1 cm transmits 80% of incident thermal neutrons, and about the same percentage of high-energy prompt gamma radiation. For gamma lines above 100 keV self-absorption is typically of minor significance. PGAA can be regarded as a matrix-independent analytical tool for samples up to a few grams. As the neutrons illuminate the samples throughout their whole thickness, the analysis provides the *average composition* of the illuminated *bulk sample*.

There are a few cases, when a special care has to be taken:

- When the sample contains a nuclide with a high neutron-capture cross section in a high concentration, neutron self-shielding may become important. However, in spectra of homogeneous samples all peak areas will be lowered uniformly by the neutron absorption, leaving the peak-area ratios the same.
- When the irradiated material contains mainly high-$Z$ elements, gamma self-absorption may become significant, especially for the low-energy gamma rays. However, above the energy of 2 MeV the attenuation of the gamma rays is almost independent of energy, which again means an approximately uniform decrease of the absolute intensities, i.e., area ratios of high-energy peaks can be used for chemical analysis without correcting for self-absorption.

The analytical result is independent of the chemical state of the elements because the analytical signal originates from the excitation of the nuclei, not the electron shells. Hence, PGAA can be used for multi-elemental *panorama analysis* without any prior information on the sample.

Since neutron and gamma fields cannot be separated, as is done in NAA, a more complex shielding is needed in this technique. This requires more construction material in the vicinity of the detector, thus increasing the spectral background induced by the scattered neutrons in these materials. (See later.)

PGAA is *nondestructive* in several ways:

- No sample preparation is necessary.
- The irradiation does not change the elemental composition of the sample. (The converted nuclei are mostly stable isotopes of the same element, and their number is at least ten orders of magnitude less than for the atoms in the sample.)

The radiation damage in the sample caused by the neutrons and gamma rays is normally negligible. If, however, charged-particle emission is induced by the neutrons, the material may undergo minor radiation damage, resulting in modifications in the chemical or crystal structure followed by discolorations. This effect may be remarkable when irradiating lithium-, boron- or nitrogen-containing samples.

Usually, the only problem requiring attention is the formation of *radioactive isotopes*. In the worst case, samples must be cooled for a few weeks until their radiation reaches the background level.

Special care must be taken, when *fissile material* is analyzed. From the gamma radiation of the original material its previous irradiation history can be determined, and this may be distorted by exposure to neutrons.

Every chemical element (except $^{4}$He) can be analyzed with PGAA. However the neutron capture cross sections vary by eight orders of magnitude (from O: 0.00019 barn to Gd: 48,800 barn). Thanks to this fact that high-cross section elements can be determined in low-cross section matrices with high sensitivity.

The main power of the method is the analysis of *light elements* (i.e., Ca and below). Their capture cross sections are characteristically a few tenths of a barn, which allows their assay even in weak neutron beams (e.g., the industrial analysis of raw materials using neutron generators). The most important of them is hydrogen, which can be analyzed with a fairly good sensitivity in almost any kind of matrix. PGAA is a unique tool for the determination of hydrogen or water content even in trace amounts.

In NAA, the samples are irradiated in an isotropic neutron field, and the induced decay gamma radiation can be detected even in contact geometry. In PGAA, neutron beams are used for activation ($10^{-4}$ to $10^{-5}$ times weaker than the activation in reactor cores), and the detector cannot be placed too close to the sample ($10^{-2}$ to $10^{-3}$ maximum efficiency). On the other hand, only a fraction of the total number of decay events takes place during the counting in NAA, decreasing the sensitivity of the method by a factor of $10^{-1}$ to $10^{-3}$ (Isenhour and Morrison 1966b), while in PGAA all prompt gamma photons can be detected with the above mentioned efficiency. All these effects result in analytical sensitivities of PGAA being lower by a factor of usually $10^{-4}$ to $10^{-6}$ compared to NAA. This deficiency can partly be overcome by using longer irradiations and larger samples. This fact, however, predestines PGAA to be primarily a major-component analytical technique (Molnár 2004).

### 31.3.2 Characterization of Prompt Gamma Spectra

The highest-energy prompt gamma lines are close to 12 MeV, unlike decay lines, which are mostly below 3 MeV. Thus, the energy range of prompt gamma spectra is much wider than that used in NAA. Prompt gamma spectra usually contain several hundred peaks. The largest fraction of the counts appears in the spectral background, not in characteristic peaks.

The complexity of prompt gamma spectra depends on the nuclear level structure of the emitting nuclide. There are two major types of spectra:

1. The lightest nuclides have no energy levels below their capture states; thus, only one prompt gamma peak appears in their spectra corresponding to the transition from the capture state to the ground state ($^{2}$H, $^{3}$H, and $^{4}$He product nuclides). The other light nuclides have a couple of levels below their capture states, so besides the direct transitions only a few others appear in the spectra ($^{7}$Li, $^{8}$Li, $^{13}$C, $^{17}$O). These spectra consist of strong prompt gamma lines (the emission probabilities are greater than 10%). The lower energy lines always sit on the Compton plateau caused by the higher-energy lines resulting in an increasing baseline toward low energies.
2. For the heavy elements another spectrum shape is typical because of the large number of possible transitions in the nuclei. The large number of overlapping peaks forms an almost smooth continuum in the mid-energy range and continuously rising with the decreasing energy (the most typical examples are Eu, Tb, and Ir). Identifiable prompt gamma peaks appear only at the low- and high-energy ends of the spectra originating from the primary and the ground-state transitions. The emission probabilities for these lines are typically a few percent only. The basic types of prompt gamma spectra are illustrated schematically in Fig. 31.1.

**Fig. 31.1**
**Typical shapes of prompt gamma spectra for the lightest (type 1) and the heaviest nuclides (type 2)**

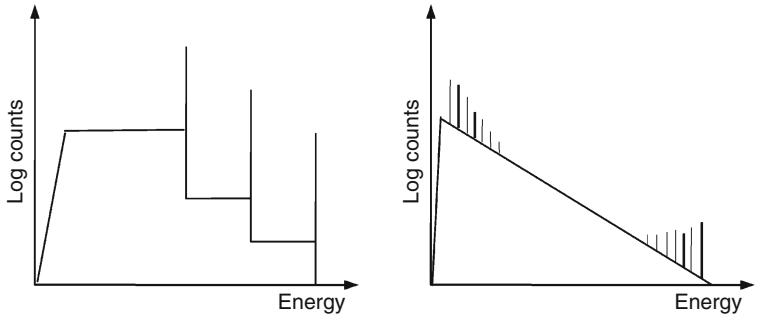


The density of the prompt gamma peaks at the high-energy end is much lower than the density at low gamma energies. Thus, high-energy peaks can be used much more reliably for qualitative analysis. When analyzing multielement samples, one can observe that the upper half of the energy range (6–12 MeV) typically contains peaks from light elements due to the energy dependence of the binding energy (Molnár 2004).

### 31.3.3 Dynamic Range and Detection Limit

Characteristic peaks always stand on a spectral background originating mainly from the Compton scattering of the higher-energy gamma photons. This Compton continuum usually contains counts that are less by two to three orders of magnitude in each channel than the area of the full-energy peak (FEP) from the gamma ray that generates it. In the case of spectra acquired with high count rates for several hours one can expect a few strong peaks with up to a few million counts, which are standing on a baseline with the height of thousands of counts per channel. In a spectrum like that a peak with the minimum area of a few hundred counts can be detected. In the everyday routine analyses, such high counts are rarely collected, so the area ratio of the strongest and the weakest peaks is typically closer to a thousand. This means that the dynamic range of the prompt gamma spectra, over which the peak areas are detectable, is three to four orders of magnitude.

From these considerations, the detectability of the elements can be estimated. In the case of a sample containing two elements only, the strongest peaks of the minor component can be at least three to four orders of magnitude smaller than those of the dominant component. This is true for the opposite case, too, so the mass ratio of any two elements can vary between six and eight orders of magnitude. For example, 0.1 mg of chlorine can be easily detected in 1 g of water (approximately 0.1 g H), and 0.1 mg of hydrogen (or 1 mg of water) can be analyzed in 0.1 g of carbon tetrachloride (containing 90% chlorine).

In spectra taken on a mixture of elements, the detection limits for components can be estimated efficiently using a few rules of thumb. The efficiency of the detector between 100 keV and 10 MeV drops by two orders of magnitude. Similarly, the minimum detectable peak area varies from a few hundreds of counts at low energies to a few counts at the highest energies. These peak areas corrected with the counting efficiency can be approximated as being constant

all over the spectrum, and that equals the minimum detectable peak area at the maximum of the detector efficiency. For the case of a high-purity germanium (HPGe) detector, the efficiency function has its maximum around 100 keV, and its value equals the geometric efficiency (see later). Based on Eq. (31.4), the *detection limit* is the following:

$$DL/\mathrm{g} = \frac{A_{\min} M/\mathrm{g\,mol^{-1}}}{0.6\,\sigma_{\gamma 0}\,\Phi_0\,\varepsilon_{\mathrm{geom}}\,t_{\max}/\mathrm{mol^{-1}}} \tag{31.9}$$

where $A_{\min}$ is the minimum detectable peak area at 100 keV, $M$ is the atomic weight of the element, 0.6 is the rounded Avogadro constant times $10^{24}$ (its unit is $\mathrm{mol^{-1}}$), $\sigma_{\gamma 0}$ is the partial gamma-ray production cross section in barns ($10^{-24}$ $\mathrm{cm^2}$), $\Phi_0$ is the thermal equivalent flux ($\mathrm{cm^{-2}\,s^{-1}}$), $\varepsilon_{\mathrm{geom}}$ is the geometric efficiency (the fraction of detected solid angle), and $t_{\max}$ is the maximum possible measurement time (s). For instance, if the minimum detectable peak area is 600 (a typical value) and the collimated detector is at a distance of about 25 cm away from the sample, then the geometric efficiency will be approximately 0.001. If the maximum measurement time is taken 100,000 s (a little longer than 1 day) and the flux $10^8$ $\mathrm{cm^{-2}\,s^{-1}}$, then using the above values and a constant with the proper unit, the estimated detection limit in micrograms can be estimated as follows (*Table 31.1*; Molnár 2004):

$$DL/\mu\mathrm{g} = \frac{M/\mathrm{g\,mol^{-1}}}{10\,\sigma_{\gamma 0}/\mathrm{b}} \tag{31.10}$$

## 31.4 Neutron Beams and PGAA Facilities

### 31.4.1 Neutron Beams

A PGAA instrument consists of a source of neutrons, a collimating beam tube to shape and direct a beam of neutrons onto a sample, a shutter to turn the beam on and off, a target assembly to position the sample reproducibly in the neutron beam, a gamma-ray detector, a beam stop to absorb the neutrons that are not absorbed by the sample, and shielding to protect the detector and personnel from neutron and gamma radiation. Each of these components will be considered in turn. The construction of a recent system illustrates clearly many of the choices involved (Robinson et al. 2009). More detailed information on the issues can be obtained in the PGAA Handbook (Molnár 2004).

To make the best analytical measurements, the PGAA beam should be both bright and clean. The neutron flux at the sample position should be high enough to obtain good counting statistics for the elements of interest in a reasonable time. Moreover, the beam should be temporally stable, spatially uniform, and contain few epithermal and fast neutrons and gamma rays so as to minimize interfering reactions and background. There should be a permanent scientist in charge of the instrument, which should be accessible to users from outside the host institution. These desiderata follow from the fundamental considerations in the previous sections.

### 31.4.2 Neutron Sources

The dominant neutron sources in laboratory PGAA are beams extracted from *research reactors*. Other neutron sources, based on radioactive nuclides or neutron generators, commonly used

**Table 31.1**

**Energy, cross section, and detection limit values according to Eq. (31.10) for the most important gamma-ray lines of each element. Decay lines are marked with an asterisk***

| El | *E* (keV) | $\sigma_\gamma$ | *DL* (μg) |
|---|---|---|---|
| H | 2,223 | 0.3326 | 0.3 |
| Li | 2,032 | 0.0381 | 18 |
| Be | 6,810 | 0.0058 | 160 |
| B | 478 | 716.0 | 0.00150 |
| C | 4,945 | 0.00261 | 500 |
| N | 1,885 | 0.01470 | 100 |
| O | 871 | 0.000177 | 9,000 |
| F | 1,634* | 0.0096 | 200 |
| Ne | 2,036 | 0.0245 | 80 |
| Na | 472* | 0.478 | 5 |
| Mg | 585 | 0.0314 | 80 |
| Al | 1,779* | 0.232 | 12 |
| Si | 3,539 | 0.1190 | 24 |
| P | 637 | 0.0311 | 100 |
| S | 841 | 0.347 | 10 |
| Cl | 1,951 | 6.33 | 0.6 |
| Ar | 167 | 0.53 | 8 |
| K | 770 | 0.903 | 4 |
| Ca | 1,943 | 0.352 | 11 |
| Sc | 147 | 6.08 | 0.7 |
| Ti | 1,382 | 5.18 | 0.9 |
| V | 1,434* | 4.81 | 1.1 |
| Cr | 835 | 1.38 | 4 |
| Mn | 847* | 13.10 | 0.4 |
| Fe | 7,631 | 0.653 | 9 |
| Co | 230 | 7.18 | 0.8 |
| Ni | 8,998 | 1.49 | 4 |
| Cu | 278 | 0.893 | 7 |
| Zn | 1,077 | 0.356 | 18 |
| Ga | 834 | 1.65 | 4 |
| Ge | 596 | 1.100 | 7 |
| As | 559 | 2.00 | 4 |
| Se | 614 | 2.14 | 4 |
| Br | 245 | 0.80 | 10 |
| Kr | 882 | 20.8 | 0.4 |
| Rb | 557 | 0.0913 | 90 |
| Sr | 1,836 | 1.030 | 9 |

**Table 31.1 (Continued)**

| El | *E* (keV) | $\sigma_\gamma$ | *DL* (μg) |
|---|---|---|---|
| Y | 6,080 | 0.76 | 12 |
| Zr | 934 | 0.125 | 70 |
| Nb | 99 | 0.196 | 50 |
| Mo | 778 | 2.02 | 5 |
| Tc | 172 | 16.60 | 0.6 |
| Ru | 540 | 1.53 | 7 |
| Rh | 181 | 22.6 | 0.5 |
| Pd | 512 | 4.00 | 3 |
| Ag | 199 | 7.75 | 1.4 |
| Cd | 558 | 1,860 | 0.006 |
| In | 273 | 33.1 | 0.3 |
| Sn | 1,294 | 0.1340 | 90 |
| Sb | 564* | 2.700 | 5 |
| Te | 603 | 2.46 | 5 |
| I | 134 | 1.42 | 9 |
| Xe | 668 | 6.7 | 2.0 |
| Cs | 176 | 2.47 | 5 |
| Ba | 627 | 0.294 | 50 |
| La | 1,596 | 5.84 | 20 |
| Ce | 662 | 0.241 | 60 |
| Pr | 177 | 1.06 | 13 |
| Nd | 696 | 33.3 | 0.4 |
| Sm | 334 | 4,790 | 0.003 |
| Eu | 90 | 1,430 | 0.010 |
| Gd | 182 | 7,200 | 0.0022 |
| Tb | 154 | 0.44 | 40 |
| Dy | 184 | 146 | 0.11 |
| Ho | 137 | 14.5 | 1.1 |
| Er | 184 | 56 | 0.30 |
| Tm | 204 | 8.72 | 2.0 |
| Yb | 515* | 9.0 | 1.9 |
| Lu | 150 | 13.8 | 1.3 |
| Hf | 213* | 29.3 | 0.06 |
| Ta | 270 | 2.60 | 7 |
| W | 146 | 0.970 | 19 |
| Re | 208 | 4.44 | 4 |
| Os | 187 | 2.08 | 9 |
| Ir | 352 | 10.9 | 1.8 |
| Pt | 356 | 6.17 | 3 |

**Table 31.1 (Continued)**

| El | *E* (keV) | $\sigma_\gamma$ | *DL* (μg) |
|---|---|---|---|
| Au | 412* | 94.0 | 0.21 |
| Hg | 368 | 251 | 0.08 |
| Tl | 348 | 0.361 | 60 |
| Pb | 7,368 | 0.137 | 150 |
| Bi | 4,171 | 0.0171 | 1,200 |
| Th | 472 | 0.165 | 140 |
| U | 4,060 | 0.186 | 130 |

in industrial applications are discussed in detail elsewhere (Alfassi and Chung 1995). Reactor neutrons originate in fission reactions at high energy, and are slowed to thermal energies by scattering from light atoms in a moderator, typically water or heavy water, surrounding the fuel. The beam is a mixture of three components: a high-energy (∼MeV) fission source distribution, a near-Maxwellian (∼meV) thermal spectrum at the moderator temperature, and an epithermal (∼eV) slowing-down region with a spectrum being approximately inversely proportional to the neutron energy. Because most neutron cross sections are inversely proportional to the neutron speed, the thermal portion is the most effective in producing (n,γ) neutron capture reactions used in PGAA. *Cold neutrons* from a cryogenic moderator are especially desirable, not only because the reaction rate per neutron is several times that of a room-temperature spectrum but also because cold neutrons can be efficiently transported by neutron guides, as will be discussed below.

The flux of neutrons normally is proportional to the inverse square of the distance from the source, so for the greatest analytical sensitivity, the sample irradiation position should be near the reactor. This is also where the gamma-ray and neutron backgrounds are highest, so care in optimizing the shielding is needed for good results. Published fluxes of reactor beams that have been used for PGAA range from $10^5$ $cm^{-2}$ $s^{-1}$ to over $10^{10}$ $cm^{-2}$ $s^{-1}$, although $10^7$–$10^8$ $cm^{-2}$ $s^{-1}$ is most common.

### 31.4.3 Shaping and Tailoring Neutron Beams

Thermal neutron beams are produced by geometrical collimation, with absorbing apertures at each end of a long flight path. A collimator does not affect the neutron energy, so the beam at the sample often contains more fast neutrons and gamma rays than desired. To improve this, the beam may pass through a filter that preferentially removes the fast neutron component and also absorbs gamma radiation. For example, 5.3 cm of sapphire in the thermal PGAA beam at NIST reduced the epithermal neutron background fivefold and the low-energy gamma ray background by an order of magnitude (Mackey et al. 2004). A number of different filter materials used in PGAA systems are listed in the PGAA Handbook (Molnár 2004).

Epithermal and fast neutrons can be eliminated entirely by using diffraction to extract a narrow range of wavelengths from the beam (Byun et al. 2002). Several orders of diffraction can be summed to increase the flux. The best beams are those from *neutron guides*, which operate by total internal reflection in a narrow channel. Neutrons incident on a surface at

angles below a characteristic critical angle are totally reflected, removing the $1/r^2$ loss with distance from the source. The critical angle depends on the material comprising the surface, and is inversely proportional to the neutron wavelength; for this reason, the guide acts as a low-pass filter. The critical angle for natural nickel is 0.7° at 6.8 Å (the most probable wavelength at the normal boiling point of hydrogen, 20 K) and 0.2° at 1.8 Å (the most probable wavelength at 300 K). Larger critical angles increase by severalfold, and hence greater transmission efficiency (which is proportional to the square of the critical angle) can be obtained with multilayer *supermirror* reflectors. Curved guides are used to avoid direct sight of the neutron source that emits also fast neutrons and gamma radiation. Reflective optical elements can increase the flux by concentrating the beam into a smaller area (Copley and Majkrzak 1989), at the expense of increased divergence. Capillary optics has been used to create a high-flux submillimeter analytical probe (Mildner et al. 2002).

### 31.4.4 Neutron Absorbers and Shielding Materials

The perfect neutron shielding material does not exist. Ideally, a shield should absorb all neutrons of all energies in a short distance without generating secondary radiation or producing residual radioactivity (Table 31.2). In practice, the most important absorbers are $^{6}$Li, $^{10}$B, and $^{113}$Cd, via the (n,α) and (n,γ) reactions. Only $^{6}$Li (and $^{3}$He) absorb neutrons efficiently without producing gamma rays. Although metallic Cd is easily shaped and an excellent absorber, neutron irradiation produces substantial residual radioactivity in addition to the strong prompt 559-keV capture gamma rays, so B and Li are preferred for high-flux tasks such as shutters and beam stops.

*Boron* has a high cross section and most of the 2.8-MeV reaction energy from neutron capture is carried by an alpha particle and $^{7}$Li recoil nucleus. However, 94% of absorbed neutrons produce a gamma ray of 478 keV. This energy is readily shielded, requiring only 4 mm of lead to reduce the radiation by half. With lithium, there is no gamma ray from the $^{6}$Li(n,t)$^{4}$He reaction, but the high-energy tritons produce about $10^{-4}$ energetic secondary neutrons per incident neutron from light elements by (t,n) reactions (Lone et al. 1980). If the

**Table 31.2**
**Characteristics of neutron-absorbing materials**

| Nuclide | Isotopic abundance, % | Cross section, b | Reaction | Product half-life and decay | Chemical forms |
|---|---|---|---|---|---|
| $^{3}$He | 0.00014 | 5,330 | (n,p)$^{3}$H | 12 years, $\beta^-$ | Gas |
| $^{6}$Li | 7.5 | 941 | (n,α)$^{3}$H | 12 years, $\beta^-$ | LiF, $Li_2CO_3$, metal, glass |
| $^{10}$B | 19.9 | 3,838 | (n,αγ)$^{7}$Li | Stable | $B_4C$, $H_3BO_3$, $Na_2B_4O_7$ |
| $^{113}$Cd | 12.22 | 20,600 | (n, γ)$^{114}$Cd | Stable | Metal |
| $^{114}$Cd | 28.73 | 0.23 | (n, γ)$^{115}$Cd | 53 h, $\beta^-$,γ | |
| $^{155}$Gd | 14.8 | 60,900 | (n,γ)$^{156}$Gd | Stable | Metal |
| $^{157}$Gd | 15.6 | 255,000 | (n,γ)$^{158}$Gd | Stable | |
| $^{160}$Gd | 21.7 | 1.51 | (n,γ)$^{161}$Gd | 3.7 min, $\beta^-$,γ | |

flux is high, the tritium produced may be hazardous. Isotopically enriched $^{6}$Li and $^{10}$B are sometimes used; 100% enrichment improves the stopping power over natural Li and B by a factor of 13 or 5, respectively.

*Lithium* carbonate and fluoride are inert and can be shaped into machinable forms. A $^{6}$Li silicate glass (Stone et al. 1994) has been used with success for collimators, beam stops, and shielding. Both carbonate and the fluoride have been mixed with polymers or paraffin to make castable (Anderson et al. 1981) or flexible neutron absorbers, but hydrogen capture gamma rays from the organic matrix can be excessive for use in the field of view of the gamma detector. The collimating aperture near the neutron source is commonly fabricated from Boral, a mixture of boron carbide and aluminum powder rolled into sheets and clad with aluminum. Where secondary radiation is of no concern (for instance shielding a detector from the last few neutrons), sheets of cadmium or boron-loaded polymer are often used. For large parts of the apparatus and for personnel protection, massive concrete in either poured or block form is cost-effective for both gamma-ray shielding and neutron shielding.

### 31.4.5 Neutron Shutter, Beam Tube, Sample Holder, and Beam Stop

It is necessary to shut the neutron beam off in order to change samples. Like the first collimating aperture, the shutter is best located close to the neutron source and surrounded by shielding, so as to minimize stray radiation at the sample position. Thermal neutron shutters are commonly made of thick boron- or lithium-containing materials, supplemented by thermalizing material or epithermal absorbers.

Neutrons are lost from the beam by scattering in air in the flight path: in passing through 1 m of air, about 5% of the neutrons are scattered into the surroundings. For this reason, it is desirable to evacuate the beam tube or fill it with helium, especially the portion outside the biological shield of the reactor. Alternatively, the beam tube can be made large in diameter and lined with $^{6}$Li absorber (Mackey et al. 2004).

Ideally, for PGAA the sample should be held in position by a material that neither absorbs nor scatters neutrons. Fluorocarbons such as **Teflon**™ Tetrafluoroethylene (TFE) or Fluorinated ethylene propylene (FEP) (both with empirical formula $CF_2$), or Teflon™ PFA (approximately $C_4F_7O$), are commonly used; in most cases, only fluorine is an important contributor to the blank spectrum. Heat-sealable FEP is available in monofilament fiber or thin film. Thin polyolefin and polyester films are readily heat sealed, but their hydrogen content can be troublesome. Low-mass samples can be suspended in the beam with fluorocarbon strings, which for most purposes add negligible background (Anderson et al. 1981). For more massive samples, a sample holder can be made of any material that does not absorb neutrons strongly or contain the elements of interest. Aluminum, magnesium, vanadium, graphite, quartz, and silicon have been used. The target chamber should be lined with a neutron absorber, preferably $^{6}$Li, to stop the neutrons scattered by the target.

Only a small fraction of the neutrons striking a typical sample are absorbed. The unused neutrons must be disposed of so that they will not endanger the experiment or the experimenters. Like the shutter, an absorber must stop the entire beam for long periods of time. A common configuration contains boron, surrounded by lead or concrete to absorb the 478-keV capture gamma ray and located out of view of the gamma-ray detector. In an unfiltered beam, the gamma rays from the neutron source must be accounted for: this component may be as important as capture in the beam stop itself.

### 31.4.6 Characterization and Monitoring the Neutron Beam

For reliable analysis, it is necessary to understand the characteristics of the neutron beam, namely its intensity (flux), spectrum, and spatial and temporal uniformity. These issues are discussed at length in the PGAA Handbook (Molnár 2004). *Foil activation* is the simplest, and perhaps the most accurate, method of measuring flux (ASTM 1998; Beckurts and Wirtz 1964). A known mass of a monitor element is irradiated for a known time, and its induced radioactivity measured with a detector of known efficiency. If the reaction rate per atom $R = \Phi\sigma$ is determined, then with the thermal cross section $\sigma = \sigma_0$ measured at 2,200 m $s^{-1}$ the thermal equivalent flux $\Phi_0$ is obtained. Gold-198 ($T_{1/2}$ = 2.7 days) is a convenient indicator nuclide, with the cross section $\sigma_0$ = 98.65 b for the reaction $^{197}$Au(n,γ)$^{198}$Au. The epithermal flux is measured by irradiating a monitor bare and another specimen of the same monitor element under a shield of cadmium to absorb the thermal neutrons. Fast-neutron (MeV) monitoring is similar, using threshold reactions that cannot be induced by slow neutrons, such as $^{54}$Fe(n,p)$^{54}$Mn. Spatial mapping can be done quickly by transfer autoradiography. A foil of In, Gd, or other readily activated material is exposed at the sample position and the induced activity detected with an X-ray film or phosphor plate. *Neutron radiography* cameras can also be used for this purpose (Hilger et al. 2006). One of two methods is generally used to measure the time stability of the neutron beam. If the reactor power is known to be stable during an analysis, the capture rate in a known standard (e.g., the 1,381.7 keV peak in a particular specimen of titanium foil) can be measured before and after each sample in order to normalize to separately irradiated standards. If the neutron source is not constant during the irradiation period, the neutron flux must be measured continuously with a neutron monitor during the time the sample is irradiated. This can be done either by measuring scattered neutrons from the beam or with a low-efficiency transmission neutron monitor.

Excellent beam quality and detector shielding can more than compensate for low neutron flux (Maier-Leibnitz 1969; Kobayashi and Kanda 1983; Matsumoto et al. 1984; Molnár et al. 1997). With careful attention to background, the sample-detector distance can be small and thus the gamma efficiency high. As a result, microgram quantities of boron have been determined in tissue with a neutron flux of only $2 \times 10^6$ $cm^{-2}$ $s^{-1}$.

Design criteria for the shielding of the gamma-ray detector in PGAA are similar to that for any gamma-ray spectrometer, with some differences due to the presence of neutrons. *Lead* is the most common shielding material for gamma rays, but it is translucent to neutrons. Even though the capture cross section is small, neutrons striking a massive shield will produce the characteristic 7,368 keV lead capture line and its Compton continuum. Reducing thermal neutron background in the detector requires an absorber outside the lead shield. Enriched $^6$Li is best in the line of sight between the sample and the detector because it does not produce extra gamma rays, and does not greatly attenuate gamma rays.

The Ge detector itself is the most convenient tool to measure both fast and thermal neutron background rates at the detector (Chung and Chen 1991). The spectrum may show a composite of the sharp 595.9 keV line from capture of slow neutrons in $^{73}$Ge and a broad triangular peak from (n,n′γ) fast-neutron excitation of the same level of $^{74}$Ge. In addition to increasing background, fast neutrons can lead to *detector damage* at a fluence as low as $10^7$ $cm^{-2}$ (Chung 1995); n-type germanium is an order of magnitude less sensitive than p-type.

In addition to the quasi-constant background characteristic of the apparatus, a variable background comes from the presence of a sample in the neutron beam. Capture gamma rays from other elements increase the continuum background under the analytical capture peak,

and may also contribute an interfering peak. Neutrons scattered by the sample itself into the apparatus may affect H, B, C, N, F, Al, Fe, Ge, and other elements (Anderson and Mackey 1993).

### 31.4.7 PGAA Facilities

PGAA has been performed at dozens of research reactors, with varying degrees of success and permanence. Since a comprehensive list was published in 2004 (Molnár 2004), new PGAA instruments have been established in Beijing (Zhang et al. 2005), Forschungreaktor München Research Reactor at Munich (FRM-II) Munich (Kudejova et al. 2008), and Oregon State (Robinson et al. 2009). Systems at Korea Atomic Energy Research Institute (KAERI) Daejon, (Cho et al. 2005a) Texas (Révay et al. 2007), and Bhabha Atomic Research Center (BARC) Trombay (Acharya 2009) have been upgraded, and a system is under construction in Lisbon (Beasley et al. 2009).

## 31.5 Samples and Standards

For a given sample material and experimental arrangement, there is an optimum sample size and shape. Samples must be large enough to give a high capture rate for good counting statistics in a reasonable measurement time but small enough to avoid inaccuracies that creep in with high counting rates. In addition, the sample should be small enough that bias from neutron absorption or scattering will be acceptably small. These considerations usually lead preferentially to small samples and long irradiation times. The composition, the experimental conditions, and the required accuracy determine what "small" means in practice.

### 31.5.1 Sample Size and Shape

Neutron self-shielding (De Soete et al. 1972; Fleming 1982; Martinho et al. 2003) and gamma-ray self-absorption (Debertin and Helmer 1988; Gilmore and Hemingway 1995) are well understood in conventional instrumental neutron activation analysis (INAA) and apply in PGAA as well. As a rule of thumb, if the thickness of the sample multiplied by the macroscopic absorption cross section (the product of element cross section and concentration summed over all components, with dimension $cm^{-1}$) is less than 0.01, then *self-shielding* will give less than 1% bias in the analytical result. Similarly, if the product of the gamma attenuation coefficient (in $cm^2\ g^{-1}$) and the mass thickness (in $g\ cm^{-2}$) is less than 0.01 then gamma *self-absorption* may be unimportant. Both self-shadowing effects are best avoided by using small samples, usually less than 1 g. However, PGAA can be performed on massive specimens, even larger than the neutron beam. Normalizing to an internal standard such as a matrix element sacrifices one degree of freedom, but need not compromise the measurement when an element ratio or mass fraction is in fact the quantity of interest. The difficult general case of large samples of unknown composition is approachable through a combination of modeling and experiment (Sueki et al. 1996; Degenaar et al. 2004).

The shape of the sample may be important, especially for hydrogenous materials such as polymers and tissues. When a sample is irradiated in a nearly parallel collimated beam of neutrons, the effects of *neutron scattering* in the sample are much greater than in the nearly

isotropic neutron field generally used for irradiations in INAA (Copley and Stone 1989; Mackey and Copley 1993). Scattering by hydrogen affects the path length of the neutrons in the sample, and therefore the probability of absorption. As a result, reaction rate is no longer proportional to the mass of analyte. The greater the scattering power of the sample (the greater the hydrogen content), the greater the bias; for instance, it is as much as 15% for 0.1 g pellets of cellulose (Mackey et al. 1991). For the most accurate work, standards are made to match the shape and hydrogen content. The shape dependence can be reduced or eliminated by making the sample spherical, or nearly so (Mackey and Copley 1993). Scattering of neutrons from the sample also increases the background from capture in the materials of the apparatus (Anderson and Mackey 1993).

### 31.5.2 Standardization

The simplest situation is a point sample, smaller than the neutron beam and with negligible mass of material to scatter or absorb neutrons or gamma rays. Most applications of reactor-based PGAA approach this ideal. The analytical sensitivity is defined as the counting rate at a certain gamma-ray energy per unit quantity of element under specified standard conditions. If the neutron flux is constant, the geometry of the system is unchanging, and the counting system is stable, the sensitivity is a constant. Two methods are in use to determine the sensitivity: using elemental standards for each element, and using fundamental parameters.

The elemental standard approach is the most straightforward, and the most tedious. A known quantity of the element of interest is irradiated under standard conditions. Standards are best prepared from pure elements or simple compounds known to be stoichiometric (Moody et al. 1988). Usually selected high-purity metals or analytical reagent grade chemicals are adequate, but a useful check is to compare multiple standards from different sources. If a suitable mass of an element cannot be accurately weighed, it may be dissolved in a suitable solvent and evaporated on filter paper. Solid standards can be diluted with an inert material such as high-purity graphite and pressed into pellets. Prepared PGAA standards may be used repeatedly for many years without change. A few exceptions have been noted: e.g., boric acid volatilizes slowly from filter paper although borax does not.

A drawback of this approach is that each element to be determined requires a separate standard. Moreover, if the experimental conditions change, for instance, a new gamma detector is installed, then each standard must be remeasured. A more robust approach is the $k_0$ *standardization* method (Molnár et al. 1998), which does not require standard samples.

If element X irradiated simultaneously with a monitor element M, then the flux cancels and the ratio of counting rates per unit mass can be written according to Eqs. (31.4) and (31.5):

$$\frac{\rho_X/m_X}{\rho_M/m_M} = \frac{\sigma_{\gamma,X}/M_X}{\sigma_{\gamma,M}/M_M} \cdot \frac{\varepsilon(E_X)}{\varepsilon(E_M)} = k_0 \frac{\varepsilon(E_X)}{\varepsilon(E_M)} \tag{31.11}$$

where $\rho$ again is the counting rate, $m$ is the mass of the component, $M$ is the atomic weight, and $\varepsilon$ is the counting efficiency at the characteristic energies of elements X and M, while $k_0$ is a constant. Values of $k_0$ and their uncertainties, relative to the hydrogen capture gamma ray at 2,223 keV, have been tabulated for more than 30,000 capture lines, (Molnár 2004; Choi et al. 2007), and are available at http://www-nds.iaea.org/pgaa. For any experimental conditions, to measure any element relative to any other element only the relative detector efficiency needs to

be calibrated. If epithermal capture is important then the equations contain other terms, but the principle is the same. A list of partial gamma-ray production cross sections ($\sigma_\gamma$) can be found in the Appendix of this volume.

Certified reference materials (CRMs), described in the Appendix such as those available from NIST (http://ts.nist.gov/), IAEA (http://www.iaea.org), BCR (http://www.irmm.jrc.be), or other national or international standards bodies, are occasionally used as multielement calibration standards. The chief drawbacks of these materials are the difficulty of selecting an appropriate material for all the elements of interest and the inferior accuracy of certified element content compared with in-house preparations. The most important use of CRMs is to validate the results of a measurement: if the certified value is obtained when a sample is analyzed in the same manner as the unknown, then the measurement is less likely to be in serious error.

As with most nuclear methods of analysis, backgrounds (peaks present in the absence of a sample) are generally small for most elements. A major goal in the design of a PGAA spectrometer is to minimize the spectral background. As with gamma spectrometry in INAA, detection limits and accuracy are impaired by a high baseline under the analyte peak. Unlike INAA, however, capture-gamma spectra contain so many transitions that the baseline can never be certain to be free of interfering peaks. A first-order background correction can be made by subtracting the signal from an empty sample container irradiated in the same manner as the sample.

However, much of the gamma-ray background counting rate is due to neutrons scattered into the apparatus by the sample. Thus, the background depends on the scattering power of the sample. Since hydrogen usually dominates the scattering, the gamma-ray background of components other than H can be estimated from the counts of the H peak. Conversely, the H background in hydrogenous samples can be estimated from the counting rate of other background components such as Al and Pb. A comprehensive listing of background lines and their origins has been published (Belgya et al. 2005).

## 31.6 High-Energy Gamma-Ray Spectroscopy

### 31.6.1 Fundamental Processes

The most important part of the PGAA facility is the gamma-ray spectrometer. The main component is the detector, which converts the energy of the gamma ray to an electronic signal. This signal is amplified, shaped, digitized, and stored in a histogram that makes up a spectrum of gamma peaks.

There are three major interactions a gamma photon may undergo in the detector (Knoll 2000):

- In the *photoelectric absorption* process, the gamma photon gives all of its energy to an electron in the detector material. The released high-energy electron creates electron–hole pairs in semiconductors or excited atoms in scintillators.
- In a *Compton scattering*, only a part of the photon energy is transferred to an electron, which then ionizes the material as it slows down, similar to a photoelectron. The Compton-scattered photon left from the scattering may interact again in the detector or may leave it.

- In *pair production*, a high-energy photon creates an electron–positron pair. Both the electron and the positron ionize the atoms of the material. After the positron slows down to thermal energy, it annihilates with an electron, creating most likely two so-called annihilation photons. The two photons have equal energies of 511 keV and fly off in exactly opposite directions. They may have further interactions.

The photoelectric interaction is the most probable process up to a few hundred keV and that is the only interaction that results in a complete absorption of the photon. Compton scattering may occur at all energies, but is the most important between a few hundred keV and a few MeV, while at high energies pair production becomes the most important interaction (see *Fig. 31.4*).

Gamma rays deposit their full energy only when the photoelectric absorption is the final step in the sequence of interactions inside the active volume of the detector, thus resulting in the full-energy peak (FEP). In Compton scattering, gamma photons having almost any energy below the initial energy can escape from the detector, causing a continuum (Compton plateau) below the FEP. Compton-scattered or escape events, however, can be identified using a guard detector annulus around the semiconductor detector. In Compton suppression mode of this guarded system the signal of gamma rays, which leave the germanium crystal (see later), are rejected. The most commonly used materials for the guard detector are sodium iodide (NaI) and bismuth germanate (BGO).

## 31.6.2 Instrumentation

### 31.6.2.1 Detector Selection

The energy range of prompt gamma radiation extends from a few tens of keV up to 12 MeV. There are two detector types in practice that are able to detect gamma rays over this wide energy range: the solid *scintillation* detector and the germanium semiconductor detector:

- Industrial applications require durable, shock-and vibration-resistant, easy-to-use equipment, which may be operated in a wide range of temperature, humidity, and pressure environments (Johansen and Jackson 2004). These criteria can be better satisfied by scintillation detectors, and such detectors may also be satisfactory for monitoring the composition of nearly identical objects.
- The superior energy resolution of the *high-purity germanium (HPGe) detectors* makes them ideal for high sensitivity analysis of samples having a large variety of compositions (Knoll 2000; Leo 1987).

In this chapter, focus is put on the spectroscopic work with HPGe detectors. There are two types of HPGe crystals; they differ in the donor or acceptor concentration. In the case of n-type detectors, the outer surface is doped with acceptor atoms, typically boron, with a thickness of a few micrometers. They have been shown to have much better resistance against neutron damage than p-type detectors, doped with a thicker layer of acceptor atoms (Knoll 2000). For the measurements of low-energy gamma radiation planar detectors are used, while in PGAA the larger-volume (at least 100 $cm^3$) closed-ended coaxial detectors are preferred (Knoll 2000; Leo 1987) (see *Fig. 31.2*). The germanium crystal has to be cooled to liquid nitrogen temperature (77 K) when operated.

**Fig. 31.2**
**Schematic shapes of planar and closed-ended types of high-purity germanium (HPGe) detectors. Thick lines show electrode connections**

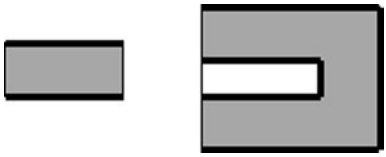

To increase the ratio of the full-energy signal relative to the Compton continuum, the simplest way is to increase the volume of the germanium detector. The suppression, however, is not proportional to the volume as often thought. The peak-to-background ratio improves approximately with the square root of the volume (Heath et al. 1999). There is another serious limitation, too: the width of the active, depleted volume can extend only for about 2–3 cm. The longest crystals commercially available these days are about 9-cm long, which are the best choice for the detection of high-energy gamma rays at present. The efficiency of charge collection of larger detectors is worse than for the smaller ones. Therefore, smaller detectors have better resolutions at low energy; however, at about 1.3 MeV, the difference practically disappears.

### 31.6.2.2 Electronics and Its Characteristics

**Analog electronics.** The number of electron–hole pairs produced in the absorption of gamma photons is in the order of hundred thousands. The induced extremely low current has to be amplified before further signal processing. There are two types of *preamplifiers*:

- The Resisitve-capacitive feedback (RC-feedback) type produces exponentially decaying signals with decay times of around 50 μs.
- The transistor-reset preamplifiers (TRPs) generate continuously increasing step-like signals, which have to be reset before reaching an upper limiting voltage level. TRPs are supposed to handle high count rates better.

The signal, whose amplitude is carefully maintained to be proportional to the energy of the impinging radiation, is digitized by an analog-to-digital converter (ADC) and the digitized result is sorted in a multichannel analyzer (MCA), then stored in a computer for further analysis. This is the traditional scheme of signal handling.

**Digital signal processing (DSP).** Digital spectrometers have been available in the market for more than 10 years (Jordanov et al. 1994). The simplest device replaces the spectroscopy amplifier and the ADC. The preamplifier signal enters and digitized data leave the module, which can be directly fed to an MCA. The desktop models integrate the functionality of the high-voltage supply, spectroscopy amplifier, the ADC, and the MCA. The common factor in all of these digital signal processors is that the preamplifier signal is conditioned and a fast sampling ADC digitizes the signal flow in real time. The stream of numbers passes through digital filters, which determines the amplitude and detection time of the signal pulse and the processor generates the corresponding channel numbers for energy or time.

There are two types of digital filters continuously processing the data stream coming from the preamplifier. The filtering process involves the calculation of sums of the digitized data using different weighting factors.

- A fast filter with the total duration of a few hundred nanoseconds is used for the detection of the events, for monitoring pileup, and yields the detection times.
- A slow filter is used to determine the step height of the preamplifier signal, which carries the energy information.

Among other advantages, the DSP manufacturers provide evidence that the temperature and long-term gain stability is much better for the DSP systems than for analog systems. Due to the shorter shaping process, the DSP systems show better high-count rate properties than the analog systems. The throughput and energy resolution also show better characteristics. However, Szentmiklosi et al. (2005) found that in wide energy range applications such as PGAA, there are still problems to be solved.

**Dead time and pileup.** All detector systems have a certain characteristic time period required to process an event. The detector system may or may not remain sensitive during this period. In the second case, events arriving during this characteristic resolution time will be lost, while in the first case, they may pile up and change the measured value, so generating a count in a different channel, and thus both events will effectively be lost. The time period during which incoming events are lost is called the dead time. To avoid a significant distortion of the number of events occurring, the count rate must be kept sufficiently low. A maximum of a few ten thousand counts per second can be handled by systems available at present. The dead time is influenced by all components of the detector system (Gilmore and Hemingway 1995).

Taking into account the dead time of a detector system is very important when an absolute intensity experiment is performed. All ADCs estimate the dead time, however their accuracy is sometimes questionable. Digital spectrometers are supposed to estimate the dead time accurately, since the time of the signal processing is exactly prescribed.

The simplest way to determine the overall dead time is to measure it using a pulser. The pulser signals should be connected to the preamplifier of the detector, using a pulse amplitude greater than that from any expected capture photon. From the known rate of the pulser and the recorded number of pulser counts, the number lost due to the dead time can be determined. The best performance is obtained with counting a radioactive source or a random time pulser together with the sample (Knoll 2000).

The *pileup* of events occurs when a second signal arrives at the amplifier within its resolution time, i.e., within the shaping width of a single pulse (typically 2–3 times the peaking time for RC-feedback preamplifiers). The piledup pulses then produce one count with an amplitude somewhere between that of the smaller event and the sum of the two event amplitudes (Gilmore and Hemingway 1995) depending on the response of the ADC to the distorted signal. When using an analog amplifier, this effect can be reduced if the *pileup rejection* mode is switched on. When a second event is detected by a fast discriminator during an adjustable inspection interval, a gating pulse is generated to inhibit the storing of the original pulse. This feature can effectively reduce the level of the continuum in the spectrum. DSPs also handle pileups: signals processed by the slow filter are rejected, if the fast filter registers additional events.

### 31.6.2.3 Response Function of Germanium Detectors

In PGAA, the energy spectrum is collected by a multichannel analyzer (MCA). The spectral shape for a single gamma ray of a given energy is called the response function. Its shape depends on the size of the germanium detector, the spectrometer electronics, the gamma-ray energy

**Fig. 31.3**

**The normal and Compton-suppressed spectra of $^{24}$Na with the gamma energies of 1,369 keV and 2,754 keV, as measured in Budapest. The features marked with numbers are listed in the text**

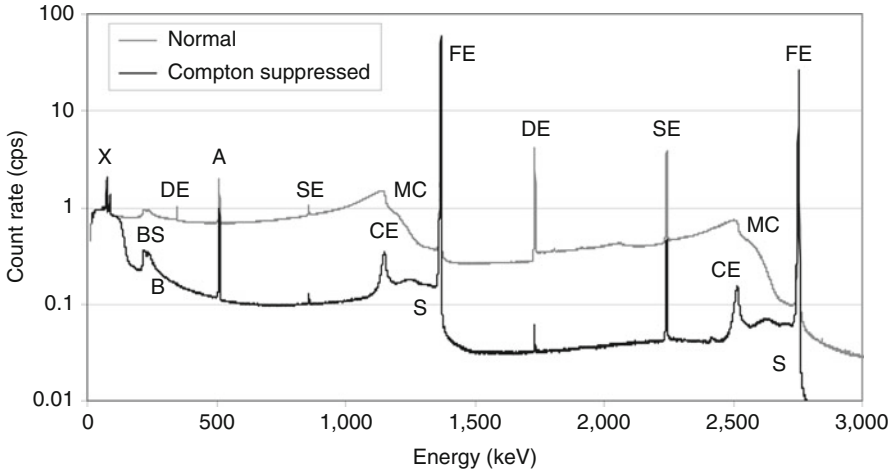


itself, and the surrounding materials. *Figure 31.3* shows the response function in the case of counting $^{24}$Na with a 25% HPGe detector in normal and in Compton-suppressed modes.

The following components could be identified in the spectrum. (Some of the events can be more easily identified in a Compton-suppressed spectrum.)

FE Full-energy peak (FEP), when the photon loses all its energy ($E$) within the active volume of the detector.

S Step below the full-energy peak, when the photons lose a small amount of energy in a small-angle Compton scattering in the collimator or in the dead region of the detector followed by full absorption of the scattered photon.

MC Multiple Compton scattering region below the full energy peak and above the Compton edge.

CE Compton edge about 220–250 keV below the full energy peak. It is a result of a single Compton-event and corresponds to the highest energy left in the detector in a single scattering. The Compton edge is below the FEP with an energy of $E/(1 + E/255.5$ keV), as calculated for free electrons.

CP Compton plateau is formed, when the Compton photon leaves the detector.

SE, DE Single and double escape peaks are 511 and 1,022 keV below the full energy peak of high-energy photons that can produce an electron–positron pair. These peaks are produced when one or both annihilation photons leave the detector.

CF Between the single escape peak and the Compton edge there are events from single escape processes. The escaping 511 keV photons may produce a Compton scattering before leaving the sensitive volume. Even a peak due to back scattering of the annihilation photon from the cold finger can be identified at the energy of $E - 341$ keV (i.e., below the FEP). This component is stronger for high-energy photons.

AE Between the single escape and double escape peaks there are events from Compton scattering of both escaping 511 keV photons, which leave the sensitive volume. Their

Compton edge is 170 keV below the single escape peak. Sometimes a back-scattered peak of one of the escaping 511 keV photons can be identified at 341 keV below the single escape peak (too weak to see in Fig. 31.3).

A Annihilation peak at 511 keV, when an annihilation radiation produced in the surrounding structural material or the sample is detected.

BS Back scattering peak at 220–250 keV is produced when back-scattered Compton-photons from the sample chamber and other structural materials in front of the detector are observed. [The exact energy is $E/(1 + E/255.5\ \text{keV})$.] In the special case plotted in Fig. 31.3 there are two back scattering peaks according to the two gamma energies, while in the typical prompt gamma spectra it covers a wider region.

B The strongly increasing background intensity toward low energies comes from the *bremsstrahlung* from photo- and Compton-electrons and also from the beta particles emitted by radioactive nuclides. A large amount of shielding material placed next to the detector may also increase the baseline at low energies due to gammas from the multiple Compton scattering in the shield (called buildup). The slope of this region can be especially steep, when the spectrum contains intense high-energy components.

X Characteristic X-ray peaks also show up below 100 keV from the shielding and other structural materials.

In case of strong pileup or random coincidences, any combinations of the above events can happen, which produce double or higher-order Compton edges or peaks at summed energies of full energy peaks. These random coincidences and peak summing must be distinguished from the true coincidence summing of gamma rays from cascades (Molnár 2004).

### 31.6.3 Calibration Procedures

The gamma spectrum is a set of counts sorted into channels, which correspond to gamma energies absorbed in the detector. This histogram must be converted into a gamma activity versus energy relationship for the determination of the reaction rate. The activities can be derived from peak areas using the *counting efficiency*. The transformation of channel numbers into energy values is called energy calibration. In the simplest linear energy calibration, one determines the channel positions of two gamma-ray peaks with accurately known energies. To obtain accurate energy data over the whole PGAA spectrum, one usually needs a correction for *nonlinearity* of the counting system. The energy *resolution* is an important quantity giving the peak width as a function of energy. It must be well known to determine the peak areas with high reliability.

#### 31.6.3.1 Energy Resolution

The energy resolution of HPGe detectors is a very important quantity. Its deterioration warns the user of the onset of various problems in the spectrometer system. The peak resolution of a HPGe-based spectrometer depends on three factors (Owens 1989):

- $W_d$: the statistical fluctuation in the number of electron–hole pairs created by gamma radiation of a given energy. It is a property of the HPGe crystal. Its standard deviation is proportional to the square root of the gamma-ray energy (Knoll 2000).

- $W_x$: there is a statistical fluctuation in the charge collection, which depends linearly on the gamma-ray energy and is also a property of the HPGe crystal. This term is neglected in most calculations, though experiments with various detectors clearly show that the term is significant, especially at high energies.
- $W_e$: the electronics has a constant noise, which does not depend on the energy. Part of the electronic noise is superposed on the signals after the amplification and thus, when using a low-gain setting, this component becomes significant (Szentmiklosi et al. 2005).

The total width $W_t$ has the following form:

$$W_t = \sqrt{W_d^2 + W_x^2 + W_e^2} = \sqrt{aE + bE^2 + c} \tag{31.12}$$

For characterization of the width of gamma peaks, the so-called full width at half maximum (FWHM) is used. For a Gaussian peak shape, the FWHM = 2.3548 $\sigma$, where $\sigma$ is the standard deviation. Another quantity can be derived in a similar way, the full width at tenth of maximum (FWTM), FWTM = 4.2919 $\sigma$ for Gaussian shapes. Thus, the FWTM/FWHM ratio equals 1.8226 for a pure Gaussian peak. The so-called Gaussian ratio implemented in certain data acquisition programs equals 0.5487·FWTM/FWHM, which is greater than unity, when the peak has a tailing.

### 31.6.3.2 System Nonlinearity

The components of the spectrometer have a more-or-less linear response to the energy, which enables the use of a simple two-point energy calibration in most applications. However, there are small deviations from linearity of the order of $10^{-3}$, which can be of great importance in PGAA because of the very wide energy range covered. Most data acquisition softwares offer the possibility of a parabolic energy calibration based on three data points; but for precise spectroscopic work over a large energy span, this may not be accurate enough.

The major source of the nonlinearity is the **ADC**. In fact, it has been observed that the shape of the nonlinearity depends only slightly on the gain settings. The most accurate way of determining the nonlinearity of the spectrometer is based on the measurement of calibration sources with well-known energies (Helmer et al. 1971). The nonlinearity of the spectrometer can be quantified as the difference of the measured peak position, $\Delta P_i$, from a linear function, which is determined by a two-point calibration based on two distinct peaks of the calibration source:

$$\Delta P_i = P_i - P_{low} - \frac{E_i - E_{low}}{s} \qquad s = \frac{E_{high} - E_{low}}{P_{high} - P_{low}} \tag{31.13}$$

where $E_i$ is the energy of the $i$th peak taken from the literature, $P_i$ is the measured channel number for the same peak, and $s$ is the slope of the two-point energy calibration line. The nonlinearity is thus a channel-dependent function, which is zero at the two calibration points by definition. Two nonlinearity functions are regarded as equivalent when they differ only in their constant and linear terms. The same nonlinearity curve can be used for slightly different gains. This is a large advantage compared to the nonlinear energy–dependent functions, (as done with the parabolic energy calibration).

The typical nonlinearities cause only a small energy difference when the amplifier gain is high, which can be neglected in low-energy gamma spectroscopy (e.g., NAA). However,

a typical nonlinearity of one-two channels may cause an energy difference of more than 1 keV at the low gains used in PGAA, which makes the peak identification impossible, and thus the application of the nonlinearity correction is vital.

**Radioactive and (n,γ) sources** with accurately known energies should be used for the determination of the nonlinearity, e.g., $^{152}$Eu, $^{133}$Ba, and $^{110m}$Ag. The $^{35}$Cl(n,γ) capture lines extend the energy range up to 8.9 MeV (Krusche et al. 1982). Above this energy, there are no better data than those of $^{14}$N(n,γ) (Jurney et al. 1997); however, the identification of prompt gamma peaks are not problematic in this energy range. A method has been developed by Fazekas et al. (1999) to fit an overall nonlinearity function with polynomials to separately measured data sets.

### 31.6.3.3 Detector Efficiency

To determine reaction rates from the gamma spectrum, the analyst has to know the counting efficiency of the detector, i.e., the ratio of the number of recorded pulses to the number of gamma rays emitted by the source. For germanium detectors, this depends on several factors, the most important of which are the geometry and the gamma-ray energy.

There have been many attempts to determine the absolute detector efficiency ε from various calculations. For instance, a *semiempirical formula* has been derived by Freeman and Jenkins (1966) and has been successfully applied by Owens et al. to HPGe detectors (Owens et al. 1991). This function was successfully fitted to the measured full-energy efficiency data (Molnár et al. 2002b), see *Fig. 31.4*.

**Fig. 31.4**

**The plot of the semiempirical efficiency functions for the Budapest spectrometer. The lines represent the individual effects, which build up the full-energy efficiency**

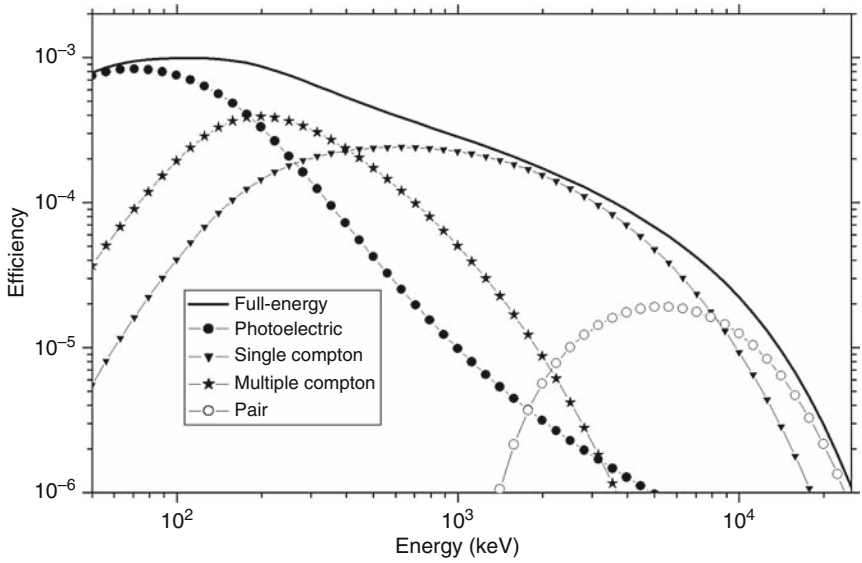

The model has a large number of parameters, so its use in the routine analysis is inconvenient. However, it emphasizes some important characteristics of the efficiency function, e.g., the slight efficiency decrease around 500–600 keV, which explains why the linear approximation on a log–log plot cannot be used in an accurate spectroscopic work.

It is preferable to measure the efficiency using gamma-ray sources with known disintegration rates [activity or reaction rate for (n,γ)-sources]. The corresponding formula is

$$\varepsilon(E_\gamma) = \frac{C_\gamma}{NP_\gamma} K = \frac{R_\gamma}{AP_\gamma} K \tag{31.14}$$

where $C_\gamma$ is the measured net peak area (counts), $R_\gamma$ is the count rate, $N$ is the number of disintegrations, $A$ is the activity, $P_\gamma$ is the emission probability of the corresponding gamma ray, and $K$ contains all the correction factors for losses during the acquisition of gamma-ray events, such as dead time and coincidence summing (Molnár et al. 2002b).

In PGAA, the sample-to-detector distance is usually large, which makes the summing of true and random coincidences negligible.

When determining mass ratios in PGAA, it is sufficient to use only the relative efficiency. During its determination, it is not important to know the accurate source activity, and it is also insensitive to the uncertainty in the source positioning. Thus, the *relative efficiency* can be determined with a higher accuracy.

In Eq. (31.14), $\varepsilon$ will depend on the attenuation of gamma rays in the layers between the sample and the detector (e.g., neutron shielding). Therefore, it is important to calibrate the detector system efficiency with the same arrangement that is used for the measurements on unknowns.

Just as in the determination of the nonlinearity, the best way to perform an accurate efficiency calibration is to measure the sources separately. To cover the whole energy range used in PGAA, it is necessary to combine data from several measurements involving both *isotopic multi-gamma sources and capture reactions* (Molnár et al. 2002b). The data sets from different sources must be normalized together at overlapping energy regions. The efficiency at any energy can be interpolated using either nonlinear or linear functions on a log–log scale or polynomials (Kis et al. 1998; Molnár et al. 2002b):

$$\ln \varepsilon(E) = \sum_{i=0}^{n} a_i (\ln E)^i \tag{31.15}$$

The form of Eq. (31.15) is flexible enough to follow the curvature of the efficiency over a wide energy range (Molnár et al. 2002b). The parameters of the polynomial can be determined from a least-squares fit to the count rates versus energy.

In many cases, the full detector efficiency can be factorized into intrinsic and geometric efficiencies. The *intrinsic efficiency* is the ratio of the number of recorded pulses to the number of gamma rays incident on the detector surface, which depends on the interactions between the gamma photons and the material of the detector, as discussed above, while the *geometric efficiency* equals the fraction of the gamma rays reaching the detector relative to the emitted ones.

**Collimated detectors.** In contrast to unshielded detectors, collimated detectors show a strong dependence of the counting efficiency on the position of the sample (Debertin and Helmer 1988). The gamma rays can reach a shielded detector only by passing through a *collimator* channel. The range of sample positions over which the detector can be seen from the sample is determined by the dimensions of the collimator $a$, $b$, and $r$ (see *Fig. 31.5*). The normal viewing solid angle is determined by the radius of the rear collimator hole and the distance $a$ +

**Fig. 31.5**

**Layout of the collimated detector, and the transmission geometry of the collimator (0 – the geometric center, *a* – sample-to-shielding distance, *b* – thickness of the collimator, *r* – radius of the collimator, *e* – end of the partial illumination region, *d* – the distance of the inner aperture to the sample). In the middle, the thick line shows the geometry factor, increasing from 0 to 1 in the transitional regions. The hatched circle represents the view of the front collimator aperture as seen by the source point. The empty circle is the source point view of the rear aperture (drawing is not to scale)**

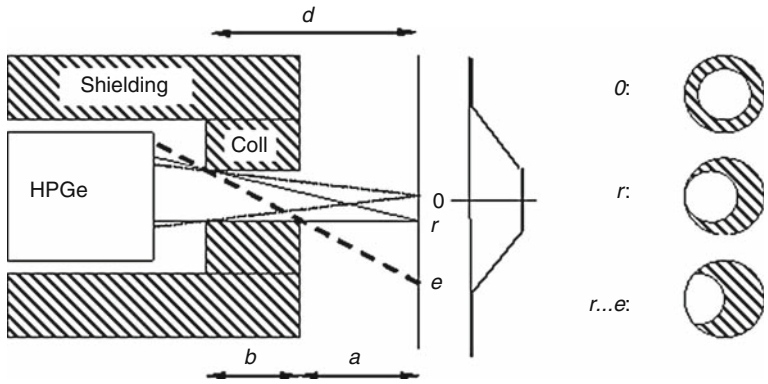


*b* of this hole from the sample. This result remains valid for any sample position for which the rear aperture is not obscured by the front wall of the shielding, i.e., at sample positions 0 to *r*. High-energy radiation may also be partially transmitted through the shielding around the apertures, increasing the effective solid angle and thus the geometric efficiency.

If a point source is moved along the line in front of the detector, its detected activity will follow the bold curve (the so-called geometry factor) in the middle of the figure. In the geometrical center ("0"), the point source illuminates the detector with the highest possible intensity (dotted lines in Fig. 31.5). The source can be moved slightly in the vicinity of the center without changing the illumination of the detector. The observed intensity is constant within the interval from $-r$ to $+r$ (thin lines in Fig. 31.5). Starting from the position *r*, the collimator partly shades the detector, and fully covers it at position *e* (thick dashed line in Fig. 31.5). The length of the partial illumination zone depends mainly on the ratio of *a* to *b*:

$$e = r + 2r\frac{a}{b} \tag{31.16}$$

The geometry factor is unity in the center, and decreases to zero in the interval from *r* to *e*. The decrease can be well approximated with a straight line (see the right side of Fig. 31.5). If the source is further away from the shielding than the thickness of the collimator, the *partial illumination zone* is longer than the constant region in the middle (Molnár 2004).

**Active and effective volume of the sample.** When measuring bulk (finite size) samples, one detects the different points of the sample with different geometry factors, which may affect the observed intensity. In the case of homogeneous samples, it is useful to introduce two quantities, the active and the effective volumes. The first one is the actual volume of the sample from where photons are emitted and may reach the detector, while the latter one is the integral of the geometry factor over the whole radiating (active) volume of the sample. Because of the

partial illumination zone, these volumes can be significantly different and may be much greater than the volume simply estimated from the projection of the collimator (Molnár 2004).

### 31.6.3.4 Determination of Spectral Background

The background means any gamma rays that do not arise from the sample under investigation. The lower the background, the lower are the detection limits. That is why it is important to fight for lower background, though it is usually a tedious process.

The origins of the background can be divided into two components. One of them is the *room-background*, which is always present. The other component is present only when the neutron beam is on (the so-called beam-background).

The room-background data discussed here are based on a week-long measurement performed using the Compton-suppressed HPGe detector in Budapest (Belgya et al. 2003; Belgya et al. 1997; Révay et al. 2004). The majority of the peaks originate from the *natural radioactive decay* chains, i.e., the $^{232}$Th, $^{238}$U, $^{235}$U, $^{237}$Np series, and $^{40}$K. These nuclides are in the construction materials of the building.

The other peaks come from the continuous activation and excitation by the different-energy neutrons induced by the *cosmic rays* of the surrounding shielding and structural materials, like aluminum, fluorine from Teflon and $^{6}$LiF-containing shielding, and even excitation and activation of the germanium in the detector and in the BGO. The evidence for inelastic scattering of fast neutrons in the PGAA detector comes from the presence of the so-called germanium triangles in the room-background spectra. *X-rays* are also observed from the lead shielding and bismuth of the BGO anti-Compton shield surrounding the detector, which are results of the interaction between them and cosmic muons (Nunez-Lagos and Virto 1996).

Some other radiations observed have special explanations for their origin. One part of these radiations is the gamma radiation coming from long-lived **$^{207}$Bi** in the BGO that is an isotopic impurity in the elemental bismuth used in the manufacturing process (Lindstrom 1990). The **$^{60}$Co** gamma rays may originate from activation of $^{59}$Co in the iron structure by slow neutrons. Again, the long lifetime makes it a persistent background component.

The total room-background rate for a well-shielded PGAA detector system may be below 1 cps, similar to the performance of a well-shielded low-background experimental set-up (Lindstrom et al. 1990), while the rate is about 100 cps for the unshielded detector.

The *beam-background* can be investigated using a high-purity heavy water ($D_2O$) sample, as a dummy target. This background spectrum contains peaks from radiation emitted by the nearby structural materials after excitation by the scattered neutrons, as well as the gamma rays from the constituents of the sample holder. The nitrogen capture lines also appear if the sample chamber is not evacuated. The Li and C peaks probably originate from the plastic neutron shielding (which contains $^{6}$Li), while the Al, Pb, Fe, and Sb peaks probably come from the structural materials.

When the germanium detector is not shielded well enough against slow neutrons, the material of the crystal can also be activated. As a result, prompt and decay gamma peaks of germanium isotopes appear in the spectrum. The relative intensities of germanium peaks in this case will be completely different from those of a germanium sample because of the almost complete true coincidence summing of gamma-ray cascades inside the detector. The prompt gamma peak at 596 keV is a clear sign of the prompt activation of the germanium detector by neutrons leaking through the detector shielding (Belgya et al. 2005).

Besides gamma peaks, the $\beta^-$ spectra from the decays of $^{75}$Ge with the maximum energy of 1.2 MeV and with a half-life of 83 min, and of $^{77}$Ge ($E_{\beta max} = 2.2$ MeV, $T_{1/2} = 11.3$ h) can be seen. The $\beta^-$ particles are in coincidence with the detected decay gammas from the daughter isotopes, partly shifting the **$\beta^-$ spectrum**. Under steady-state operational conditions one count in the 139.7 keV peak from $^{75m}$Ge indicates about two counts of $\beta^-$ decay from the 83 min half-life isotope, and similarly one count in the 159.7 keV peak from $^{77m}$Ge accompanies about two counts from the 11.3 h half-life isotope. The conclusion is that one has to wait several days to make low-background measurements with detectors exposed previously to slow neutrons.

Gamma peaks identified as arising from inelastic scattering of fast neutrons on various materials are coming from fast neutrons generated after slow-neutron capture on light elements (Li, B in slow-neutron shielding materials) (Lone et al. 1980). Thus their relative yields depend strongly on the shielding materials. The lowering of this component is the most difficult part of the construction of the shielding, due to the large penetration power of fast neutrons and the diffuse nature of their sources. The most important signals from the (n,n′) reaction on the germanium detector (the germanium "triangles") appear at 596 and 692 keV, and less significant triangles at 834, 563, and 1,039 keV.

### 31.6.4 Compton-Suppressed Spectrometers

Compton-suppressed spectrometers, as mentioned earlier, are used to decrease the Compton plateau associated with all peaks in the spectrum. The Compton shielding also suppresses the single- and double-escape peaks. The most frequently used setup consists of a main germanium detector, which is surrounded by one or more scintillators, with the exception of an aperture where the radiation enters. (There is also another hole at the back or at the side for the insertion of the germanium detector into the suppressor.) The annulus detects gamma rays scattered out from the germanium detector. To minimize the rate from the external radiation, the detector system should be placed into a thick lead shielding. When, due to a Compton event, the photon transfers only a portion of its energy to the germanium detector, and the resulting Compton photon is caught by the *scintillator*, the registration of the detector signal can be prohibited by an anti-coincidence gating. The most efficient Compton suppressor systems can reduce the Compton plateau by more than an order of magnitude.

The annulus serves both as an active and a passive shielding for the germanium detector. The annular guard detector is often made of sodium iodide [NaI(Tl)] or *bismuth germanate* ($Bi_4Ge_3O_{12}$ or BGO). The BGO has higher gamma-ray detection efficiency than the cheaper NaI(Tl), and so is frequently used in PGAA.

There are two basic layouts of Compton-suppressed detector systems.

- In the simpler *coaxial arrangement*, the cylindrical surface of the germanium detector is fully covered by the scintillator. More sophisticated layouts partly cover the flat surfaces in the front and in the black, as well. In the latter geometry, only a small solid angle of the forward and of the backward scattering directions is not shielded (see *Fig. 31.6*).
- In the *perpendicular geometry*, the scintillator is placed coaxially with the direction of the detection, while the germanium detector is placed at right angles to it. Thus the detector observes the photons from the side, through the hole in the scintillator facing the source, and the forward scattered photons are caught behind the germanium detector by the scintillator.

**Fig. 31.6**
**Coaxial and perpendicular Compton-suppressed detector systems**

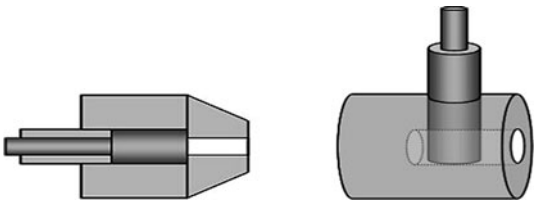

**Fig. 31.7**
**Normal and Compton-suppressed spectra of a nitrogen-containing compound (deuterated urea)**

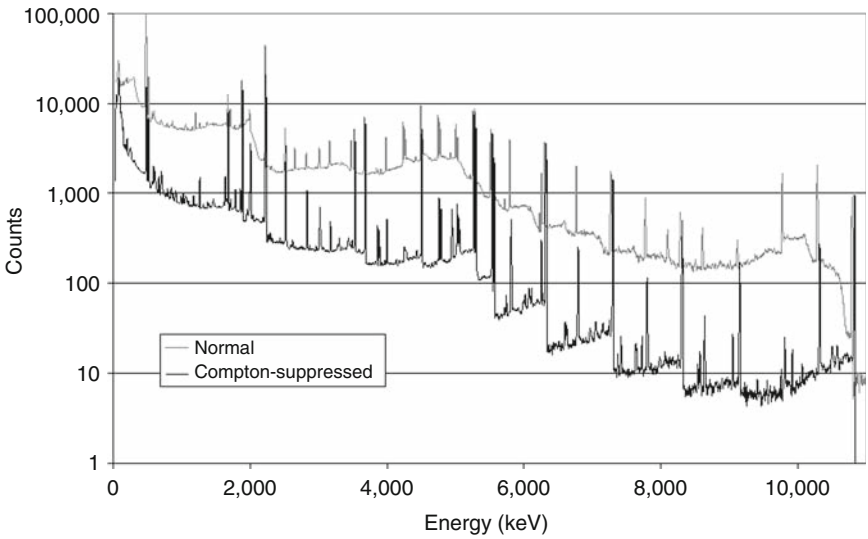


The perpendicular arrangement preserves more from the shape of the normal spectrum, which may be disadvantageous. The response function of the coaxially arranged HPGe–BGO detector system is simpler by being effective at suppressing the smooth continuum and in many cases the suppression is also better.

Typical normal and Compton-suppressed spectra are shown in *Fig. 31.7*.

## 31.6.5 Other Sophisticated Detection Solutions

### 31.6.5.1 Composite Germanium Detectors

Composite detectors are relatively new developments in gamma-ray spectroscopy. They make possible the tracking of gamma rays inside the detector. The clover detector has four closely placed germanium crystals arranged like the leaves of a four-leaf clover. The cluster detector has

seven segments; one of them is in the center (Wilhelm et al. 1996). Both of these detector types can also be surrounded by a BGO guard detector. The advantage of this arrangement is that a part of the Compton photons leaving one detector may be detected in a neighboring one. These scattered signals can be used for Compton suppression, but it is better to add them up for the purpose of getting back the original peak energy (Elekes et al. 2003).

#### 31.6.5.2 Coincidence Techniques

The usefulness of $\gamma$–$\gamma$ coincidences in elemental analysis was pointed out by Ehmann and Vance (1991). The simplest coincidence setup consists of two germanium detectors (Ember et al. 2002). In coincidence mode, the two detectors detect two gamma rays that are emitted in fast consecutive decays of an excited nucleus. By doing this, the spectrum can be greatly simplified at the expense of a low coincidence count rate. Single-step (non-cascading) gamma rays can be greatly suppressed together with their Compton continua.

Another way to improve the coincidence detection efficiency is the utilization of gamma-ray detector arrays. This has been proposed and used by the Material Science Group at JAERI (Hatsukawa et al. 2002).

#### 31.6.5.3 Chopped-Beam PGAA

The purpose of a beam chopper is to turn the beam on and off periodically. The separation in time of prompt and decay gamma transitions by means of a beam chopper was suggested in the pioneering work of Isenhour and Morrison (1966a, b), and more recently by Zeisler et al. (2001), with the aim to identify spectral interferences in the prompt spectrum from the decay gammas.

One of the simplest beam choppers is a rotating disk partially covered with neutron-absorbing material. $^{6}$Li-loaded plastic is ideal for prompt gamma measurements because it produces no background gammas resulting in a *pulsed neutron beam*. When a neutron pulse hits the target, it activates the sample just like the continuous beam. The gamma spectra are detected in both the prompt and the pure decay phases. As a result, one can consider the chopped-beam measurement as a combination of PGAA and cyclic NAA (Szentmiklosi et al. 2006a). The decay peaks of certain short-lived nuclides can be measured in a chopped neutron beam with detection limits of about an order of magnitude better than normal PGAA (Szentmiklosi et al. 2005).

## 31.7 Spectrum Evaluation

Accurate and reproducible evaluation of prompt gamma spectra is of great importance, as the sample composition is determined from the evaluated peak areas. At different energies in a typical prompt gamma spectrum, the height of the baseline and the peak areas may differ by several orders of magnitude. The peaks are asymmetric, their shapes, especially their widths, depend on the energy, and may also depend on the count rate, and the peaks sometimes appear in complex multiplets. It is not infrequent that more than 1,000 peaks can be identified in

a prompt gamma spectrum. The minimum requirement an evaluation software must meet to be applicable in PGAA is the ability to fit at least ten peaks in one region of interest (ROI), and to have the asymmetric built-in function that describes HPGe peaks under extreme conditions. It must be able to evaluate most of the peaks automatically, but it should allow manual fitting whenever needed in difficult cases. Only a few of the evaluation software available on the market can handle this extraordinary task.

Many softwares are capable of fitting only a few peaks in each region. *Peak shapes* are often fit with only the symmetric Gaussian curve, or in some cases with a curve combined from a Gaussian and an exponential decay at the low-energy side, joining smoothly to each other. But many of the features, appearing in typical PGAA spectra cannot be handled using these simple algorithms. One of the most successful approaches is the Hypermet algorithm developed at the Naval Research Laboratory in the 1970s (Phillips and Marlow 1976a, b), which was further developed into PC-based and later into Windows-based, user-friendly programs, and now also involve the calibration routines (energy, efficiency, and nonlinearity correction) (Fazekas et al. 1997).

Peaks are fit in regions wherever the counts exceed the average level of the baseline significantly. The counts in the regions are described as the sum of peaks, peak-dependent background terms, and a parabolic baseline. A peak consists of a symmetric and an asymmetric part, usually a low-energy tailing:

- The symmetric part of the peak is described by a Gaussian. Its width $W$ depends on the energy: $W = (a + bE)^{1/2}$.
- The asymmetric part of the peak, called the *skew term*, is intended to describe the effects of the improper charge collection. It is an exponentially modified Gaussian (EMG) function, i.e., an exponential term with a constant decay parameter convoluted with a Gaussian function having a width of $W$. The amplitude of the skew term is proportional to the whole peak area (Révay et al. 2001b).

The sum of these two components makes up a peak, while the sum of their integrals equals the peak area.

Peak-dependent background is a step-like shape below the peak, which consists of a rounded step due to small-angle Compton scattering and a tailing component:

- The step is described by the convolution of a Heaviside function (i.e., a unit step function) shifted to the peak and a Gaussian function (with the same width as the peak). This rounded step is thus described with an erf function, whose inflection point is at the peak energy. Full-energy peaks have reverse steps, their height is in the order of a few thousandths of the peak area (Révay et al. 2001b), while the steps below the escape peaks increase toward the high energies. The step height of a single escape peak is almost negligible, and for a double escape peak it is similar to that of the full-energy peak.
- A longer tail is due to surface effects for high-intensity peaks. It is also described by an EMG function, but with a longer decay.

The peaks sit on a baseline described by a second-order parabola. A *right skew* may also appear, especially in the case of strong peaks in the low-energy region. In many cases, this component can be eliminated by adjusting the pole/zero setting of the amplifier (in the case of RC-feedback preamplifiers), at the cost of slightly increasing the easily treatable left skew.

The positions of the peaks can be calculated as the centers of gravity

$$\langle E \rangle = \frac{\int_{-\infty}^{\infty} E(j)P(j)\,\mathrm{d}j}{\int_{-\infty}^{\infty} P(j)\,\mathrm{d}j} \tag{31.17}$$

where $j$ is the serial number of the channel, $E(j)$ is the energy, while $P(j)$ is the count number in the channel. The above peak shape and its fit to measured data points for two very different single isolated peaks are shown in Fig. 31.8.

The peaks are more asymmetric at high energies, i.e., a substantial fraction of their areas come from the skew. The Gaussian ratio, as defined earlier, is usually about 1.1–1.6 depending on the energy. Low-energy, strong peaks may show further asymmetries compared to the ideal Gaussian shape: e.g., the skew term may increase with increasing count rate.

**Fig. 31.8**

**Prompt gamma peaks of nitrogen at 1,885 and 10,830 keV**

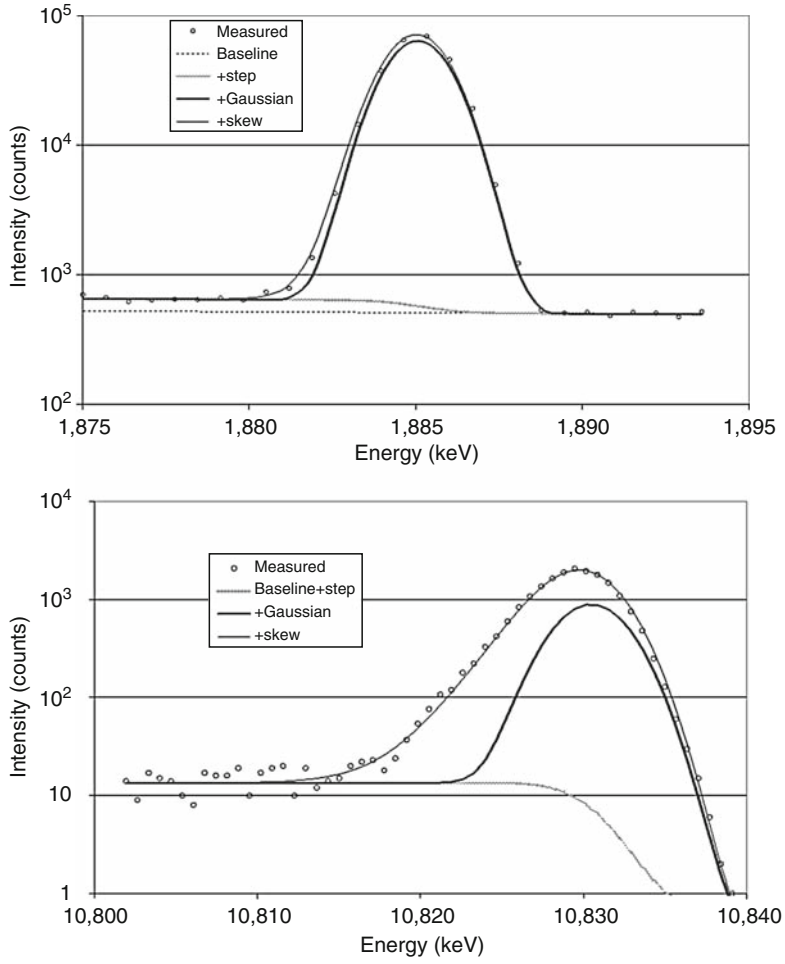

The increase in the peak width as well as the amplitude and slope of the skew term over time is a natural consequence of detector *aging*, and can be tracked by the periodic calibration of these parameters. The appearance of a long left skew and a significant, irremovable right skew can be signs of the damage to the semiconductor crystal, which can temporarily be fixed by adjusting the pole/zero in the RC-feedback preamplifier.

In the case of single peaks with shapes that cannot be described using the model built into the evaluation software, the simple *peak summing* method can be used for the determination of their areas. Peak summing (as described in Gilmore and Hemingway 1995) must be performed carefully especially in the case of asymmetric peaks. The region of the summing must be defined symmetrically around the peak maximum, so the background value subtracted using a linear interpolation will not be significantly different from the one using a step function. In the case of peaks with extremely good statistics, peak summing can also be more helpful than fitting, since the minor deviations from the model function may become significant. The uncertainty of peak area determined this way can be simply calculated from the Poisson statistics of the channels involved, i.e., $A \pm \sqrt{(A + B)}$, where $A$ is the net peak area after background subtraction, $B$ is the background, so $A + B$ equals the total counts in the examined region. This method can be used for single peaks only.

The most important non-electronic process that results in distorted peaks is the *Doppler broadening* of gamma lines due to the recoil of the emitting nucleus (see Sect. 31.2.1). This broadening usually can be corrected with a slightly increased width parameter during the fit; however, in some cases the evaluation programs fit complicated multiplets. The two most prominent representatives of this effect in prompt gamma spectra are the annihilation peak, and the *boron peak* from the $^{10}B(n,\alpha\gamma)^{7}Li$ reaction. While the first one is not used for analysis, the second one is one of the most frequently analyzed peaks in PGAA. Its shape highly depends on the composition of the matrix through the degradation constant (Szentmiklosi et al. 2007a).

## 31.8 Quantitative Analysis

During quantitative analysis, the masses of certain components and the composition of the sample are determined using peak areas and spectroscopic data. There are two approaches for quantitative analysis: absolute and relative.

### 31.8.1 Absolute Approach

In the absolute method, the masses of certain components are determined. Assuming thin samples, peak areas are directly proportional to the masses, so the mass can be determined from nuclear constants and the conditions of the measurement based on Eq. (31.4) as follows:

$$m = \frac{M}{N_A} \frac{A}{\varepsilon(E_\gamma)\, t\, \sigma_{\gamma 0}\, \Phi_0} \tag{31.18}$$

where $M$ is the atomic weight, $N_A$ is the Avogadro constant, $A$ is the net peak area, $\varepsilon(E_\gamma)$ is the counting efficiency at a characteristic gamma-ray energy of the given nuclide, $t$ is the measurement time (live time), $\sigma_{\gamma 0}$ is the partial gamma-ray production cross section, and $\Phi_0$ is the thermal equivalent neutron flux. The flux can be determined as described in Sect. 31.4.6, or by measuring a known amount of any element with a known partial cross section.

The analytical sensitivities (count rate per unit mass) can also be determined for any PGAA facility using standards with known masses of components. According to the most frequently used procedure a flux monitor is irradiated first, and the peak area is corrected with the ratio of the monitor values as measured during the analysis and the determination of the sensitivity.

In the case of the absolute method of PGAA the sample has to be weighed, and the concentrations of the detected components can be determined as the ratios of their masses compared to that of the sample. So the accuracy of the final result depends on two measurements, the mass determination with PGAA and the weighing of the sample.

The absolute method can be used with high accuracy, if the following criteria are met:

- The mass of the sample is known accurately. (The sample is chemically stable, and it does not contain unknown amount of absorbed water, etc.)
- The sample has to be close to the ideally thin case, i.e., no significant self-absorption or self-shielding corrections are necessary, and neutron scattering does not affect the result either.
- The flux profile is uniform across the neutron beam and the flux is stable in time.
- The dead-time correction of the spectrometer is accurate in the given count rate range. This is necessary to obtain the accurate live time.
- Samples are measured always in the same geometry using the same detector (i.e., the efficiency does not change).

### 31.8.2 Relative Approach

In the relative method, the components are determined from a single measurement on one sample. Instead of the masses, the mass ratios of the components are determined to avoid the mentioned corrections and other possible sources of error, whether or not the above criteria are fulfilled. Following the idea of the $k_0$ standardization (see Eq. (31.11)) the mass ratio can be expressed as

$$\frac{m_1}{m_2} = \frac{A_1}{A_2}\frac{\varepsilon(E_2)}{\varepsilon(E_1)}\frac{\sigma_{\gamma 2}}{\sigma_{\gamma 1}}\frac{M_1}{M_2} \tag{31.19}$$

where $A$ is the net peak area, $M$ is the atomic weight, $\varepsilon(E)$ is the counting efficiency, $\sigma_\gamma$ is the partial gamma-ray production cross section, and subscripts 1 and 2 represent two different chemical elements and their characteristic energies. The equation needs the determination of the peak areas, the counting efficiency, and then the mass ratio can be determined using the partial cross sections from a spectroscopic database (Révay 2009).

The determination of mass ratios is not sensitive to the variation of the neutron flux or the improper dead-time correction. For homogeneous samples, the inhomogeneous flux profile and the neutron self-shielding do not affect the result either. Gamma-ray self-absorption can be neglected in many cases, though it can distort the results when irradiating thick samples and if peak areas at both low and high energies are used in the calculation. When using peaks with the energies above 2 MeV, as mentioned in Sect. 31.3.1 this effect can also be neglected even in the case of bulk samples.

Relative and absolute methods can be used simultaneously, but the analyst has to keep in mind that mass ratios have lower uncertainties than the mass values. The uncertainty calculation is described in detail by Révay (2006).

In many cases, all major and minor components of the sample can be detected using PGAA with a reasonable accuracy. (The total amount of trace elements has to be negligible compared to the uncertainties of the concentration values.) In this case, the concentrations of the constituents can be determined as the ratios of the masses and their sum. The sum of the calculated masses is biased with the same systematic errors as the individual masses; thus, their ratios will be unbiased like the mass ratios (Révay 2009).

Even when it is the dominant component of the sample, oxygen can only be determined with a low accuracy. In the case of minerals, concrete or glasses and many natural inorganic materials the amount of oxygen can be best determined from stoichiometry (Révay 2009).

## 31.9 Applications

Since the establishment of PGAA in the 1970s as a nuclear method for multielement quantitative analysis, there have been several reviews of PGAA applications; see, e.g., (Deconninck et al. 1981) or more recently (Paul and Lindstrom 2000) and (Yonezawa 2002). In addition, there is a PGAA handbook that includes an excellent application review section by Anderson (Molnár 2004). The last of these is quite thorough and covers reactor-based PGAA applications from 1980 through 2004. Other reviews have focused on measurements of specific elements for which PGAA is highly applicable and widely used such as the review of PGAA hydrogen measurements by Paul (1997), PGAA for boron by Sah and Brown (1997) and Paul (2005), and for cadmium by Grazman and Schweikert (1991). There are also several overviews of applications and developments at specific PGAA facilities. Révay et al. (2008a) has recently published a review of PGAA activities at the Institute of Isotopes, Park et al. (2005) a review of activities at the Korea Atomic Energy Research Institute, Rios-Martinez et al. (1998) and Wehring et al. (1997) reviews of PGAA at the University of Texas, US, Yonezawa (1999) of PGAA at Japan Atomic Energy Research Institute, and Unlu and Rios-Martinez (2005) a review of PGAA at university reactors. To avoid redundancy with or duplication of these very thorough reviews that have preceded this work, this section focuses on PGAA applications developed or implemented during the past decade, focusing primarily on those of the last 5 years and refers the reader to the aforementioned reviews for historical and additional information.

There continues to be development of neutron generator-based PGAA (see, e.g., Park et al. 2009; Reijonen et al. 2004), neutron source-based PGAA (Turhan et al. 2004; Park et al. 2004), and more recently, accelerator-based PGAA (Naqvi and Nagadi 2004; O'Meara et al. 2001; Postma et al. 2007; Postma and Schillebeeckx 2005) in which resonance neutron capture is exploited for quantitative analysis. Applications of PGAA based on the use of these nonreactor neutron sources include: analysis of archeological artifacts (Postma and Schillebeeckx 2005); online bulk analysis of carbon, oxygen, and other elements (see, e.g., Lim and Sowerby 2005); portable-source PGAA detection of explosives or other prohibited materials (Dokhale et al. 2001) and detection of land mines (Miri-Hakimabad et al. 2008). Uses of portable sources include those for borehole logging for coal and ore analysis (e.g., Borsaru et al. 2004; Charbucinski et al. 2004). There has also been recent work using in vivo PGAA for determination of nitrogen as it relates to protein status (Ahlgren et al. 1999; Kasviki et al. 2007a, b; O'Meara et al. 2001). See (Morgan 2000) for a review of in vivo PGAA applications. The scope of this review has been restricted to PGAA applications using neutron beams extracted from nuclear reactors.

An analysis of recent reactor-based PGAA applications reveals that there have been a number of new developments during the past decade, and that some of the applications that helped to establish the utility of PGAA as a quantitative method continue to be implemented in both traditional and innovative ways. As has been observed for many years, there is a great deal of PGAA work performed in the fields of archeometry and geological sciences, and in the areas of hydrogen and boron analysis. During the past 5 years, innovations have included uses of PGAA in combination with other modes of analysis such as neutron imaging, improvements in instrumentation, innovations based on modifications of the neutron beams, and the development of dynamic in situ PGAA. There has also been an expansion of PGAA applications into the fields of advanced materials analysis, and fissile and explosive materials analysis. This section will begin with a description of new applications and innovations in implementation of PGAA methods, followed by uses of PGAA in fundamental nuclear chemistry, PGAA of advanced materials, element-specific applications, field-specific applications, and finally PGAA for quality assurance and reference material certification.

## 31.9.1 Innovations and Advances in PGAA Methodologies

### 31.9.1.1 In Situ PGAA

Perhaps the most noteworthy achievement of the last decade was the work by Révay et al. (2008b) in which the first in situ PGAA measurements of dynamic processes were reported. The challenges presented by dynamic, in situ PGAA measurements are not trivial and include difficulties arising from neutron capture background signals, achieving timing resolution that is consistent with the process, and limitations in amount of signal for a given time window. In this work, uptake of hydrogen by palladium catalysts was observed dynamically by using PGAA to monitor the hydrogen to palladium element ratios. The significance of the new PGAA method has been described as it relates to the process of hydrogenation in catalysts in a recent paper by Teschner et al. (2008).

### 31.9.1.2 Neutron Focusing

Some of the recent innovations in PGAA involve the use of neutron optics to increase the intensity of the beams used to interrogate the sample. Over the past 2 decades, focused beams of neutrons have been used to provide greater neutron flux density on the sample, thereby enhancing neutron absorption reaction rates (Chen-Mayer et al. 1999; Mildner and Chen-Mayer 1999). Applications of focused beams in PGAA continue to appear in the literature, though are typically limited to analyses of high absorption cross section materials or major element components of a material. Chen-Mayer et al. (2000) achieved threefold PGAA sensitivity gains using multi-capillary lenses. These focused beams combined with prompt gamma-ray spectrometry were used to detect and quantify the amount of a number of elements in a variety of materials, including boron in Standard Reference Material (SRM) 611 Trace Elements in Glass, and iron and chromium in SRM 160b Stainless Steel. For this work, the samples were larger than the focal spot, so the reaction rate gains were not commensurate with the gain in neutron current density. Neutron current density gains of a factor of 40 were

achieved at this same facility using a monolithic lens and the sensitivity for a gadolinium beam enhanced by a factor of 34 (Chen-Mayer et al. 2001). Focused-beam PGAA was used to determine the radial distribution of residual chlorine in high-purity quartz cylinders formed from flame hydrolysis of silicon tetrachloride (Chen-Mayer et al. 2003). This information in combination with NAA results for total chorine content was used as the basis for comparison with XRF results. Neutron focusing systems at the same facility were used by Swider and Walters (2004) to evaluate the utility of this approach in analysis of paint pigments and metals. Hils et al. (2004) used parabolic guide tube to increase neutron intensity, achieving a sixfold gain in neutron intensity; the authors predicted that gains of several orders of magnitude could be achieved by multiplexing. More recently, Segawa et al. (2008) achieved two-dimensional compositional mapping of cadmium wire figures with spatial resolutions on the order of a millimeter with a focused and collimated neutron beam.

#### 31.9.1.3 PGAA and Neutron Diffraction and Imaging Methods

Additional innovative developments in PGAA, pioneered by scientists from the Institute of Isotopes, Budapest have been achieved through hybridization of PGAA with other neutron-based analytical methods such as neutron imaging and diffraction. Kasztovszky et al. (2007) developed the combination of time-of-flight neutron diffraction and PGAA to provide compositional and structural information on ceramic and metal samples. Pulsed neutrons from a spallation source were used to investigate the utility of performing PGAA to provide compositional information in combination with neutron diffraction studies (Kasztovszky et al. 2008d). This was further developed in a very elaborate combination of neutron and X-ray tomography to locate samples in thick, opaque containers (Kasztovszky et al. 2008c). Belgya et al. (2008) constructed an instrument, which combined PGAA and neutron tomography to provide both compositional information and imaging results.

#### 31.9.1.4 Chopped Beams

Chopped or pulsed neutron beams have been used to improve signal-to-noise ratios in PGAA spectra and to extend the breadth of analytical capabilities by combining PGAA with short-lived NAA, allowing detection and quantification of a larger number of elements from the same experiment. Zeisler et al. (2001) demonstrated the use of coincidence counting with a chopped neutron beam to eliminate the 472-keV gamma-ray interference arising from neutron capture by sodium from the Doppler-broadened gamma ray accompanying neutron capture by $^{10}B$, improving the ability to determine boron in biological systems.

More recent work implementing chopped neutron beams includes a number of applications performed at Budapest. Chopped neutron beams were used in conjunction with measurements designed to determine gamma-ray production cross sections (essentially, the neutron absorption cross section multiplied by and gamma yield) and $k_0$ values for short-lived nuclides used for conventional (delayed) neutron activation analysis (Révay et al. 2003, 2005; Szentmiklosi et al. 2006a). This work was developed further with improvements in the chopper controller to improve the precision and provide simultaneous acquisition of prompt and delayed activation analysis spectra (Szentmiklosi et al. 2007b). The combined PGAA/INAA system was applied to analysis of relatively large samples (several grams) of sodium iodide in

which PGAA and the delayed spectra were used for determination of sodium, iodine, scandium, thorium, and thallium (Szentmiklosi et al. 2008).

#### 31.9.1.5 PGAA in Highly Absorbing Samples or Containers

There has long been utility in performing PGAA for quantitative analysis of materials that cannot be subjected to conventional INAA. A subset of these is strongly absorbing materials. Such materials are typically prohibited from the in-reactor irradiations used for conventional INAA, but not prohibited from neutron beam irradiations. Although, PGAA has very good sensitivities for strong absorbers, these materials present other challenges due to neutron attenuation within the sample. There are two basic approaches to provide accurate results in the PGAA of strong absorbers, one uses experimental data in the form of calibration curves or internal standards contained in the matrices of interest, and the other, calculations to determine correction factors. In recent work by (Acharya 2009), valid results in determination of element content of strongly absorbing samples were obtained by use of a combination of an internal standard and calibration/validation over a large range of mass fraction values of the absorber of interest, boron. A similar approach was used by Harrison and Landsberger (2009) to account for absorption by boron.

When the sample cannot be removed from the container and the container is strongly absorbing, the analysis may be even more complicated as there may be both gamma-ray attenuation and neutron absorption to consider. Révay (2008) described determination of element content of samples in thick containers, specifically the determination of noble gases in aluminum cylinders and uranium compounds in thick lead containers. Two different approaches were applied, one for which gamma-ray attenuation and neutron absorption by the container is minimal, and the other for which attenuation is significant.

#### 31.9.1.6 PGAA of Large Samples

PGAA is an attractive method for determining the average bulk element content of large samples, particularly when the size of the subsamples typically used by other more conventional analytical methods would not be indicative of the bulk composition due to material heterogeneity. However, bulk PGAA measurements present a challenge because both neutron attenuation and gamma-ray attenuation may be significant. A recent approach described by Blaauw and Belgya (2005), to account for neutron attenuation within large samples used a Monte Carlo approach to calculate correction factors for a standard sample geometry based on the absorbing and scattering power of the sample. The results from the Monte Carlo calculations were compared with experimental results for three materials and agreed favorably for correction factors on the order of 5% and 24% but were not in agreement for more strongly absorbing materials.

#### 31.9.1.7 Improvements in signal-to-noise ratio

As with all methods for quantitative analysis, improvements in signal-to-noise ratios are desirable as a means of increasing sensitivities and decreasing limits of detection. Developments

in this area include the use of digital spectrometry, coincidence and anti-coincidence counting, and sophisticated mathematical data manipulation. Improvements in signal-to-noise using Compton suppression were implemented at the PGAA facility at Korean Atomic Energy Research Institute by Cho et al. (2005a) as part of work to optimize the instrument for boron determinations. Coincidence counting was used to improve signal-to-noise in PGAA measurements of liquids containing hydrogen and boron (Ember et al. 2002) and of gadolinium tracers in borosilicate glass samples (Ember et al. 2004). Toh et al. (2008) used coincidence of two or more gamma rays as a means of improving signal-to-noise in analysis of foods and polymer materials. A very innovative approach to improving signal-to-noise was reported by Im et al. (2007), who used principle component analysis to identify and then exclude the noise component of a PGAA spectrum.

#### 31.9.1.8 Advances and Applications in $k_0$ PGAA

The use of the $k_0$ method, originally developed for INAA, has come into prominence for use with PGAA during the past decade. This method was originally developed for INAA as a means of standardization for quantitative analysis based on the use of a single comparator, efficiency curves for the detection system, and experimentally determined constants to account for characteristics of the reactor neutron spectrum for a given facility. As applied to PGAA, the $k_0$ method essentially looks at element sensitivities for a given neutron beam and detection system (efficiency curve) combination. Lindstrom (2003) recently published an overview of $k_0$ PGAA. Research performed during the past decade has included the work by Sun et al. (2003) at the Korean Atomic Energy Research Institute for determination of $k_0$ factors for non-1/$v$ nuclides ($^{113}$Cd, $^{149}$Sm, $^{151}$Eu and $^{155}$Gd, $^{157}$Gd), and by Sun et al. (2005) for determination of $k_0$ factors and partial gamma-ray production cross sections for several elements (boron, nitrogen, silicon, phosphorous, sulfur, and chlorine) commonly determined using PGAA.

Applications of the $k_0$ method in quantitative PGAA are widespread. Some specific examples include the multielement characterization of a National Institute for Environmental Studies (Ibariki, Japan) typical diet reference material (Matsue and Yonezawa 2001) and a collaboration in which scientists used INAA and PGAA for determination of element composition of environmental and food samples (Freitas et al. 2008). In the latter work, $k_0$ PGAA was performed using the method described by Révay (2006), which includes a very thorough and detailed evaluation of uncertainty. PGAA facilities, particularly those equipped with neutron beam choppers, have also been used for determination of $k_0$ factors for short-lived products of neutron activation for use in $k_0$ NAA; see, e.g., (Révay et al. 2003) and (Szentmiklosi et al. 2006a).

### 31.9.2 Measurements of Cross sections, Gamma-Ray Energies, and Emission Probabilities

The very basis of PGAA, neutron capture followed by de-excitation of the compound nucleus through emission of characteristic gamma rays, provides information on the nuclear properties of the absorbing nuclide. Careful measurements permit determination of the prompt gamma-ray production cross section, which may be decoupled into the gamma yield, and neutron capture cross section. Quantitative PGAA may be based on comparison with element standards

of known composition, or may be based on calculations involving values for the number of neutrons interacting with the sample and values for these cross sections. For this reason, there have been many experiments designed to measure these values. For example, Park et al. (2006) performed high accuracy PGAA to determine the value of the neutron absorption cross section of $^{6}$Li, and Borella et al. (2005) to determine the value for $^{209}$Bi.

A great deal of high accuracy, high precision prompt gamma-ray spectroscopy was performed at Budapest to provide values for the partial prompt gamma-ray neutron capture cross sections, as well as gamma-ray energies and intensities (Molnár et al. 2000; Révay et al. 2000, 2001a; Molnár 2004). Their compilation of results represents the most up-to-date and accurate PGAA data available. There are many examples of determinations of partial gamma-ray production cross sections for specific isotopes. For example, thermal neutron capture cross section values were published for $^{99}$Tc (Molnár et al. 2002a). In that work, it was also noted that PGAA provided order of magnitude better sensitivity than passive counting for quantitative analysis of this isotope. Extremely careful PGAA measurements to determine the intensities of the prompt gamma rays emitted from neutron capture by chromium were performed to provide more precise values than were available in the literature (Belgya and Molnár 2004). Determinations of the intensities of 36 gamma rays from $^{35}$Cl were published in order to enable energy and efficiency calibrations of germanium detection systems over the wide range of energies commonly encountered in PGAA work, i.e., from about 100 keV to 11 MeV (Molnár et al. 2004). Similar work by Belgya (2008) involved determination of the intensities of prompt gamma rays from nitrogen for which the highest energy prompt gamma ray is above 10 MeV, to permit calibration of PGAA detection systems to these energy ranges.

PGAA facilities have also been used to assist in the elucidation of nuclear structure, as de-excitation gamma rays provide information on the level structure of the absorbing nucleus. Swider et al. (1994) used PGAA spectroscopy to observe gamma-ray cascades induced by neutron capture in $^{128}$Te, indicating level structure of the $^{129}$Te product nucleus. More recent work by Walters (2009) has involved the use of a PGAA gamma-ray spectrometer to provide information on the level structures of several germanium isotopes. Investigations of nuclear parameters involving higher energy, resonant capture phenomenon have been published recently (Pallone and Demaree 2009).

### 31.9.3 Identification of Explosives and Fissile Materials

Another area in which the number of PGAA applications has grown is that of detection and identification of fissile materials. Neutron-based analytical techniques have the sensitivity and selectivity needed for the investigation of many nuclear materials. Molnár et al. (2004) described the use of chopped beam PGAA to provide both the prompt gamma neutron capture and short-lived decay spectra from uranium isotopes and the use of these values in the determination of uranium and the degree of $^{235}$U enrichment. English et al. (2004) described the use of gamma spectrometry and PGAA to characterize *legacy radioactive materials* and subsequently extended the work to include short-lived NAA as well as PGAA (English et al. 2008).

For many years, PGAA has been exploited for use in detection and identification of explosive materials, often based on the use of portable neutron sources and detection of nitrogen. Very recently, Im et al. (2009b) have applied principle components analysis to evaluation of PGAA spectra for identification and classification of explosives. Im and Song (2009a) recently published a review of PGAA applications in the detection of illicit materials.

### 31.9.4 Measurements of Advanced Materials

Measurement of advanced materials is another area in which the number of PGAA applications has been increasing steadily. The utility of PGAA has kept pace with the needs of the materials science community in the characterization of materials such as the new generations of metal catalysts, ceramics, and biopolymers. In addition, many of the recent PGAA applications have been associated with the study of hydrogen storage materials such as metal hydrides, components of hydrogen fuel cells, hydrogen-selective membranes, and other emerging energy-efficient technologies. Measurements of advanced materials that deal exclusively with determination of hydrogen or boron are covered in the subsequent sections; other recent applications in advanced materials are reviewed here.

PGAA determinations of carbon, nitrogen, and silicon were used to help ascertain the amounts of silicon nitride and silicon carbide formed by high-temperature and high-pressure processes (Balazsi et al. 2004, 2005). Results from PGAA for carbon and hydrogen in fiber epoxy composite samples were used to estimate fiber volumes based on the carbon to hydrogen ratios and comparison with samples of known fiber volume (Dorsey et al. 2004). Kasztovszky et al. (1999) determined impurities in aluminum oxides and Szentmiklosi et al. (2006b) in materials containing calcium-sulfate, as some impurities are known to affect thermoluminescence in materials used for radiation dosimetry. PGAA (together with Fourier-transform infrared spectrometry) was used in the study of another ceramic, barium titanium oxide, to distinguish residual free hydrogen from hydroxyl groups associated with moisture (Atakan et al. 2008). Contaminants also affect magnetic or electrical properties of many metal oxyanion materials; PGAA was used to evaluate levels of both dopant and impurity elements in a variety of these materials (Perry et al. 2008). Similar studies using PGAA to determine rare-earth contaminant elements were carried out on a variety of rare-earth oxides (Perry et al. 2005). In the field of biopolymers, Balazsi et al. (2009) recently used PGAA to determine element composition of biopolymer-apatite structures derived from eggshells with biodegradable coatings. And PGAA was used extensively to determine the chemical composition and water content of synthetic polymer membranes (Young et al. 2003).

Analysis of fullerenes for impurities, especially residual hydrogen has been an important component in the study of the structure and properties of these materials. Révay et al. (2006) determined the amounts of carbon and impurity elements (hydrogen, boron, and nitrogen) in $C_{60}$ and $C_{70}$ fullerenes. In a similar vein, recent work by Paul et al. (2009) involved characterization of carbon nanotube materials to determine levels of residual catalyst metals and hydrogen impurities present in commercially available materials. Other recent applications of advanced materials include the study of proton uptake in un-doped and yttrium-doped $BaPrO_3$ and compared with that in Gd-doped $BaCeO_3$ (Jones et al. 2005).

### 31.9.5 Analysis of Hydrogen

PGAA is uniquely suited for quantitative analysis of hydrogen due to the large dynamic range of the method and due to the nondestructive nature of the analysis as compared with other analytical methods, which typically rely on combustion of the sample. PGAA has been used to determine hydrogen levels ranging from a few micrograms per gram to several percent. Limits of detection for hydrogen for some representative matrices and facilities include 70 μg for coal and botanical materials at the Oregon State University PGAA facility (Robinson et al. 2009);

15 μg for geological materials at the Japan Atomic Energy Research Institute PGAA facility (Yamazaki et al. 2007); 15 μg for biological materials at the National Institute of Standards and Technology thermal neutron PGAA facility (Mackey et al. 2004); and 5 μg in palladium catalysts in Budapest (Révay et al. 2008b).

Relatively small amounts of hydrogen may affect the properties of metals, ceramic oxides, minerals, and other materials. For example, hydrogen causes embrittlement of metals, alters proton conductivity of ceramics and the physicochemical structures and melting points of minerals. There has been an enormous expansion of PGAA applications for determination of hydrogen in the materials sciences, especially those involving hydrogen storage materials, fuel cells, and other emerging energy-efficient technologies. Recent applications are presented here; for earlier work in hydrogen PGAA applications, see the review by Paul (1997).

PGAA has been used to study a number of materials, particularly light metals, to determine hydrogen storage capacity. Cao et al. (2009) reported using of PGAA to measure hydrogen in thin films that were fabricated to evaluate the H storage capacity of metal and metal alloy hydrides. Materials studied included a series of magnesium hydride thin films that had been exposed to hydrogen for different times and PGAA results were used to evaluate the optimum exposure conditions for maximum hydrogen uptake. To help determine the optimum magnesium-to-titanium ratio for hydrogen uptake, a series of thin films consisting of magnesium–titanium metal alloys with continuously varying composition were exposed to hydrogen to form metal hydrides. PGAA results indicated that the molar fraction of hydrogen increased with increasing magnesium mole fraction. Tompa et al. (2003) used PGAA to determine hydrogen in amorphous alloys containing varying amounts of nickel, copper, and zirconium. Results of PGAA in combination with those from NMR were used to evaluate hydrogen diffusion in alloys of differing compositions and to evaluate residual hydrogen in these materials. Results of PGAA were used together with those obtained from gas chromatography to determine residual hydrogen in aluminum foils and single crystals; gas chromatography was needed to supplement PGAA results due to the presence of hydroxyl-aluminum surface coating (Buckley and Birnbaum 2002).

Other studies have focused on ceramics and other materials that preferentially filter hydrogen, and on engineered catalysts for potential use in hydrogen fuel cells. Some recent PGAA measurements with direct or indirect implications for hydrogen fuel uses include the following examples. PGAA was used to determine hydrogen in platinum catalysts before and after drying to evaluate free hydrogen content, water content, and the hydroxyl component of the support structure (Kasztovszky et al. 2002). Results from quantitative PGAA of hydrogen, combined with qualitative results from other techniques including infrared spectroscopy, neutron vibrational spectroscopy, and small angle X-ray scattering were used to study hydrogen in crystalline and amorphous alumina (Paglia et al. 2004). And similarly, Atakan et al. (2008) used PGAA in combination with Fourier-transform infrared spectroscopy and thermogravimetric analysis to study effects of heat treatments on residual water in ceramic oxides and to help distinguish free hydrogen from hydroxyl groups. PGAA was used to determine amount of hydrogen sequestered by the cage compounds of microporous silicate, clathrasil decadodecasil, finding that results were consistent with those from NMR analyses, which indicated that H was released upon cage decomposition (van den Berg et al. 2007). PGAA has been used extensively by researchers at the University of Texas (US) to study proton exchange in lithium ion batteries (Aghara et al. 2005; Alvarez et al. 2007). At the same facility, Arunkumar et al. (2008) used PGAA for investigations into the structure and proton transfer properties of lithium–manganese–nickel compounds studied for potential use in lithium-type batteries.

A great deal of PGAA work on hydrogen determinations focused on facility characterization and method improvements. Chung et al. (2007) described a very thorough characterization of the PGAA instrument at the Korean Atomic Energy Research Institute, including characterization of the background spectrum and validation of the PGAA method for hydrogen quantification. Validation was accomplished, in part, using SRM 1632c Trace Elements in Coal (Bituminous), SRM 173c Titanium Alloy, and SRM 2453 Hydrogen in Titanium Alloy, demonstrating the large dynamic range for hydrogen measurements. Yamazaki et al. (2007) described a method developed for determination of low levels of hydrogen in geological standards in which samples were measured under helium gas to prevent moisture uptake. This work also involved a very careful hydrogen sensitivity calibration and characterization of hydrogen background count rates for that facility.

### 31.9.6 Analysis of Boron

PGAA is also uniquely suitable for determination of boron, in this case due to the high neutron capture cross section of $^{10}$B, and correspondingly high PGAA sensitivity. Limits of detection for boron using this technique are nearly always submicrogram and often of the order of a few nanograms, depending on the characteristics of facility (Molnár 2004). Robinson et al. (2009b) reported limits of detection of $\leq$0.6 μg for botanical materials using a thermal neutron PGAA instrument with a neutron flux of $2.8 \times 10^7$ cm$^{-2}$ s$^{-1}$ at Oregon State University, USA. Mackey et al. (2004b) report detection limits of 70 ng for biological materials using a thermal neutron PGAA facility with a neutron flux of $3 \times 10^8$ cm$^{-2}$s$^{-1}$. Byun et al. (2004) report detection limits of 67 ng at the Korean Atomic Energy Research Institute PGAA facility with a flux of $7.9 \times 10^7$ cm$^{-2}$s$^{-1}$ based on evaluation of background and sample container blanks. Detection limits may be even lower for facilities with higher neutron fluxes or more efficient detection systems. Determination of boron is nearly always included in multielement PGAA work; recent work focusing exclusively on PGAA determination of B is described here.

Some recent work determining boron by PGAA has focused on the analytical difficulty, caused by neutron attenuation, of measuring high-content boron materials (Acharya 2009; Harrison and Landsberger 2009). Others have dealt with the difficulty presented by high count rates from highly absorbing, boron-containing materials, such as the work described by Ember et al. (2001) in determining Gd in borated glasses and subsequent work using coincidence counting to improve signal-to-noise in highly absorbing material (Ember et al. 2002). Other PGAA scientists have presented methods for determining the peak area that address the difficulties associated with modeling the shape of the Doppler-broadened peak resulting from the emission of the 472-keV gamma ray from $^7$Li following the $^{10}$B(n,αγ)$^7$Li reaction (Sun et al. 2008) or the difficulty encountered when subtracting Gaussian-shaped interfering gamma-ray peaks from the Doppler-broadened boron peak (Szentmiklosi et al. 2007a; Zeisler et al. 2001). Both Sakai et al. (2005) and Yamauchi et al. (2005) interrogated the shape of the broadened boron peak to obtain information on the chemical environment of the capturing nucleus.

PGAA has been employed for quantitative analysis of boron in boron-containing tumor drugs used for boron neutron-capture therapy. To study the distribution of such drugs in the mouse model, Cho et al. (2007) determined boron in tumors and other tissues of mice that had been injected with boronophenylalanine. Accuracy of the boron determinations at this facility had been established by previous work describing the facility, element standards, and the analysis of several certified reference materials (Cho et al. 2005b). Byun et al. (2004)

determined boron in a variety of reference materials as part of work to fully characterize the diffracted polychromatic neutron beam used at the Korean Atomic Energy Research Institute.

### 31.9.7 Biological and Environmental Applications

PGAA has been used in combination with INAA (or other methods) in biological and environmental studies in which a complete (or nearly complete) compositional characterization is desired. Anderson and coworkers have used both PGAA and INAA for determination of element content of foods for the past 2 decades. Highlights have been described in a 2001 overview of that program (Anderson et al. 2001). A more recent description of quantitative PGAA of 22 elements in a variety of foods, food and dietary supplements was presented by Anderson and Mackey (2005). Similarly, Freitas et al. (2008) used INAA and PGAA for determination of element content of nutritional and environmental samples, and Oura et al. (2007) for the determination of element content of atmospheric particulate matter. Multiple methods were also used to characterize the element content of cosmetics, in which PGAA was used to determine samarium and gadolinium (Furuta et al. 2008). PGAA was used extensively to determine the nutritive elements, carbon, nitrogen, and phosphorus in cattails (Zhao et al. 2008). As part of that research Zhao and Robinson (2009) presented a comparison of results obtained using cold and thermal neutron beams, noting the differences in the effects of hydrogen and sample thickness on element sensitivities.

### 31.9.8 Archeometry

PGAA has been used extensively over the years, alone or in combination with INAA or other methods, for multielement analysis of archeological specimens or artifacts. In many cases, the artifact or specimen may be unique and, therefore, not expendable. Even when destruction of a portion of the artifact is acceptable, the sample or specimen may be difficult to analyze using methods that require sample dissolution. For either INAA or PGAA, multielement analysis can be achieved without sample dissolution, fusion or other destructive methods used to introduce the sample into the detection device and PGAA has the added advantage of inducing little residual radioactivity. PGAA is often used to provide scientists with information on the element composition without lasting harm to the specimen. And, if necessary, artifacts analyzed by PGAA may be subsequently subjected to further analyses by other methods. Biro (2005) published an overview of PGAA applications in this field; and Lehmann et al. (2007) presented a discussion of neutron-based analytical and imaging techniques for investigation of cultural and archeological artifacts. Selected recent applications of PGAA in archeometry are described here.

In archeometry, element compositional data are often used to determine provenance and to assess artifact age. Results from multielement $k_0$ PGAA of a variety of artifacts ranging from ceramics to bronzes were used to ascertain provenance and assist in determining specimen ages (Sueki et al. 1998; Oura et al. 1999). PGAA was used to determine metal contents of several bronze and silver artifacts (Kasztovszky et al. 2000) and ancient silver coins (Kasztovszky et al. 2005). The provenance of Iron-Age bronze artifacts was evaluated based on PGAA determinations of major element and selected trace element content (Rogante et al. 2007). Copper-to-zinc ratios and the lead content of organ reed pipes determined by PGAA, combined with historical information concerning the use of these metals in the components of reed

pipes, allowed researchers to estimate the dates of the artifacts (Manescu et al. 2008). Ceramic figurines created by Amerindian peoples in the Los Roques Archipelago prior to the arrival of Europeans were investigated by PGAA; major and minor element contents were used to assist researchers in determining provenance (Kasztovszky et al. 2004). Results from a similar study of Amerindian pottery artifacts from Venezuela were used to ascertain provenance and support the hypothesis that seasonal migration established relationships among communities from different locations (Sajo-Bohus et al. 2005, 2006). A large number of samples from stone tools and associated source materials were analyzed to determine geological classifications of the materials and assess provenance of the tool artifacts (Kasztovszky et al. 2008a, b). Major element and selected trace element contents determined by PGAA of prehistoric stone tools were used to distinguish tools made of green schist from those of blue schist (Szakmany and Kasztovszky 2004).

PGAA has been an integral part of European "ANCIENT CHARM" project (Analysis by Neutron resonant Capture Imaging and other Emerging Neutron techniques: new Cultural Heritage and Archeological Research Methods; http://ancient-charm.neutron-eu.net/ach) since its inception in 2006. The research associated with this project has contributed innovations in the method, and the information provided by PGAA measurements has contributed to the knowledge of the art and archeological artifacts studied. Two PGAA instruments, one at the Budapest Research Reactor (Hungary) and the other at the FRM-II Reactor in Garching (Germany), have been used for element determinations in a variety of cultural and archeological objects. Results from PGAA have been used alone or in combination with neutron diffraction for two-dimensional structural information or with neutron tomography for three-dimensional material characterization. The characteristics of the Prompt Gamma Activation Imaging (PGAI), or prompt gamma activation imaging facility at FRM-II reactor were described by Kudejova et al. (2008a). The characteristics of the Budapest PGAA instrument were described by Révay et al. (2004, 2008a). In development of a method to combine PGAA with time-of-flight neutron diffractometry, test samples were fabricated and analyzed as described by Kasztovszky et al. (2008c). Applications of PGAA in the Ancient Charm project have included the analysis of metal-based artifacts such as brass plates, bronze sculpture, tin–lead implements (Kasztovszky et al. 2007), and investigations of copper, limestone, bronze, and glass artifacts (Kasztovszky et al. 2008d).

### 31.9.9 Characterization of Geological Materials

PGAA has been used extensively over the years for multielement analysis of geological materials, in part, because geological materials may be difficult to analyze using methods that require sample dissolution and because PGAA has very good sensitivity for some elements of interest in these materials such as rare-earth elements, which are often used to distinguish the source or origin of geological materials. For example, (Perry et al. 2002) used PGAA to determine mass fraction values for 25 elements in metal sulfides and silicate rocks formed by processes at oceanic geothermal vents. The rare-earth elements were used to infer the relationship of the materials to specific geothermal field locations. More recently, Cristache et al. (2009) used PGAA and epithermal NAA to determine mass fractions of nine elements in Black Sea sediments, results of which were used to confirm the geological origins of the sediment.

Ebihara and Oura (2001) assessed the use of PGAA at the Japan Atomic Energy Research Institute for element analysis of extraterrestrial materials obtained from space missions; of

particular interest was evaluation of any residual activity and the potential perturbation of isotopic ratios that would interfere with subsequent analysis by other techniques. Evaluation indicated that PGAA was suitable in light of all considerations. More recently, Kudejova et al. (2009) reported on the feasibility of using PGAA for multielement determinations in Allende meteorite specimens.

The presence and amount content of boron in volcanic materials has been determined using PGAA in several studies conducted by Gmeling et al. (2005) and used to infer degree of fluid enrichment in magmatic materials. These researchers investigated both boron and chlorine but found boron to be most suitable as a predictor for fluid enrichment. They followed this work with PGAA studies of volcanic materials from several locations around the globe (Gmeling et al. 2007a) and from the East Carpathian Volcanic Field (Gmeling et al. 2007b). Similarly, Marschall et al. (2005) reported determination of element content of high-pressure metamorphic rocks, finding that results from PGAA compared well with those from other methods. Marschall et al. (2009) also evaluated boron and chlorine as predictors of dehydration in geological materials. Miyoshi et al. (2008) used PGAA for multielement determination of volcanic specimens (basalts) and found that ratios of boron to rare-earth element help to establish geological source information.

### 31.9.10 Quality Assurance and Analysis of Reference Materials

PGAA data obtained from experiments conducted at well-established facilities have been used routinely as benchmarks against which results from other techniques or newer facilities are evaluated. In the development of newer facilities and instruments in which PGAA is combined with other methods, analytical results were benchmarked against results obtained from the Budapest PGAA facility Kudejova et al. (2005). Sandor et al. (2002) have described a study for determination of major element composition of ancient coins, in which PGAA results were used as the benchmark to evaluate results from a newly developed Energy Dispersive X-Ray Fluorescence (EDXRF) method. In addition, in similar work involving PGAA and EDXRF of Roman silver coins, PGAA results were used as the benchmark (Kasztovszky et al. 2005). Results from PGAA were used by Kvardakov et al. (1998) as a benchmark against which to compare results from neutron incoherent scattering for H determinations. Similarly, hydrogen concentrations in a titanium alloy were determined by neutron incoherent scattering and compared against results obtained from cold neutron PGAA (Perego and Blaauw 2005).

Another of the traditional uses of PGAA has been that of a complementary technique to INAA and other analytical methods in certification of reference materials (Lindstrom 1998; Ihnat 2000). Use of PGAA allows certification of light elements such as hydrogen, boron, nitrogen, and some rare-earth elements such as Gd and Sm that are not easily accessible by other analytical techniques. Depending on levels present, PGAA may contribute results for many more elements in certification campaigns. Some recent applications of PGAA as applied to certification of reference materials are presented here. The materials and elements determined are presented to provide a sense of the breadth and depth of PGAA capabilities. There are no doubt additional instances in which PGAA results were used in the certification of reference materials. However, due to the routine nature of many of these analyses, results of certification analyses are included only in the certificates of analysis, and may not be found in the peer-reviewed literature.

In the analysis of biological materials, PGAA is often used to determine light elements. For example, Anderson (2000) reported use of PGAA to determine mass fractions of H, B, C, N, Na, Cl, K, and S for certification of these elements in SRM 1946 Meat Homogenate. Matsue and Yonezawa (2001) reported use of PGAA to determine H, B, C, N, Na, S, Cl, and K in a National Institute of Environmental Studies (NIES) typical diet reference material. Zeisler et al. (2008) reported on the certification of SRM 1577c Bovine Liver in which PGAA contributed values for H, N, K, and S. Other measurements of certified reference materials include determination of N in a variety of NIST biological and geological Standard Reference Materials (Paul 2001). Both INAA and PGAA data accumulated over more than 10 years were used to assess stability of two biological reference materials, SRM 1566a Oyster Tissue and SRM 1547 Peach Leaves (Mackey and Spatz 2009).

For analyses of geological and environmental reference materials, PGAA may be used to measure both major element constituents (as well as light elements) and trace amounts of boron, cadmium, and rare-earth elements. Dyar et al. (2001) used PGAA to determine boron in a variety of reference minerals. Mackey et al. (2007) reported certification of SRM 695 Multi-Nutrient Fertilizer in which PGAA was one of several techniques used to certify mass fractions for 17 elements and provide reference or information values for another seven elements. PGAA contributed to certified or reference values for B, Cd, Fe, K, Mn, and N in this material. More recently PGAA was used in certification measurements for three soil SRMs (2709a, 2710a, 2711a) contributing results for B, Cd, Fe, Gd, K, Mn, Si, Sm, and Ti in these materials. Paul et al. 2009, Mackey and Spatz 2009, Sieber et al. 2007 reported certification of major and minor element constituents of SRM 57b Silicon Metal for which PGAA was used to provide results for B, Al, Ti, Mn, and Fe. Miura et al. (2008) employed PGAA for determination of boron in National Measurement Institute of Japan ceramic certified reference materials using chlorine and silicon as internal standards in developing calibration curves for boron in this matrix.

## References


Acharya R (2009) J Radioanal Nucl Chem 281:291

Aghara SK, Venkatraman S, Manthiram A, Alvarez E (2005) J Radioanal Nucl Chem 265:321

Ahlgren L, Albertsson M, Areberg J, Kadar L, Linden M, Mattsson S, McNeill F (1999) Acta Oncol 38:431

Alfassi ZB, Chung C (1995) Prompt gamma neutron activation analysis. CRC Press, Boca Raton

Alvarez E, Biegalski SR, Landsberger S (2007) Nucl Instrum Meth B 262:333

Anderson DL (2000) J Radioanal Nucl Chem 244:225

Anderson DL, Mackey EA (1993) J Radioanal Nucl Chem 167:145

Anderson DL, Mackey EA (2005) J Radioanal Nucl Chem 263:683

Anderson DL, Failey MP, Zoller WH, Walters WB, Gordon GE, Lindstrom RM (1981) J Radioanal Chem 63:97

Anderson DL, Cunningham WC, Capar SG, Baratta EJ, Mackill P (2001) J Radioanal Nucl Chem 249:29

Arunkumar TA, Alvarez E, Manthiram A (2008) J Mater Chem 18:190

ASTM (1998) Standard practice for determining neutron fluence, fluence rate, and spectra by radioactivation techniques (E261), Report E 261-98. ASTM International, West Conshohocken

Atakan V, Chen CW, Paul R, Riman RE (2008) Anal Chem 80:6626

Balazsi C, Cinar FS, Kasztovszky Z, Cura ME, Yesilcubuk A, Weber F (2004) Silic Indus 69:293

Balazsi C, Cinar FS, Addemir O, Kasztovszky Z, Kover Z, Weber F (2005) Size effects in micro- and nanocarbon added C/Si3N4 composite prepared by hot pressing. In: Dusza J, Danzer R, Morrell R (eds) Fractography of advanced ceramics Ii. Trans Tech, Zurich-Uetikon, pp 238–241

Balazsi C, Bishop A, Yang JHC, Balazsi K, Weber F, Gouma PI (2009) Compos Interfaces 16:191

Beasley DG, Alghamdi A, Freitas MC, Fernandes A, Révay Z (2009) J Radioanal Nucl Chem 281:307

Beckurts KH, Wirtz K (1964) Neutron physics. Springer, Berlin
Belgya T (2008) J Radioanal Nucl Chem 276:609
Belgya T, Molnár GL (2004) Nucl Instrum Meth B 213:29
Belgya T, Révay Z, Fazekas B, Héjja I, Dabolczi L, Molnár G, Kis J, Östör J (1997) The new budapest capture gamma-ray facility. In: Molnár GL, Belgya T, Révay Z (eds) Proceedings of the 9th international symposium capture gamma-ray spectroscopy and related topics. Springer, Budapest, pp 826–837
Belgya T, Révay Z, Ember PP, Weil JL, Molnár GL (2003) The cold neutron PGAA-NIPS facility at the Budapest Research Reactor. In: Kvasil J, Cejnar P, Krticka M (eds) Proceedings of the 11th international symposium on capture gamma-ray spectroscopy and related topics. World Scientific, Singapore, pp 562–568
Belgya T, Révay Z, Molnár GL (2005) J Radioanal Nucl Chem 265:181
Belgya T, Kis Z, Szentmiklosi L, Kasztovszky Z, Festa G, Andreanelli L, De Pascale MP, Pietropaolo A, Kudejova P, Schulze R, Materna T (2008) J Radioanal Nucl Chem 278:713
Biro KT (2005) J Radioanal Nucl Chem 265:235
Blaauw M, Belgya T (2005) J Radioanal Nucl Chem 265:257
Borella A, Moens A, Schillebeeckx P, Van Bijlen R, Molnár GL, Belgya T, Révay Z, Szentmiklósi L (2005) J Radioanal Nucl Chem 265:267
Borsaru M, Berry M, Biggs M, Rojc A (2004) Nucl Instrum Meth B213:530
Buckley CE, Birnbaum HK (2002) J Alloy Compd 330:649
Byun SH, Sun GM, Choi HD (2002) Nucl Instrum Meth A487:521
Byun SH, Sun GM, Choi HD (2004) Nucl Instrum Meth B213:535
Cao LR, Hattrick-Simpers JR, Bindel R, Tomlin BE, Zeisler R, Paul R, Bendersky LA, Downing RG (2009) J Radioanal Nucl Chem. doi:10.1007/s10967-009-0058-y
Charbucinski J, Duran O, Freraut R, Heresi N, Pineyro I (2004) Appl Radiat Isot 60:771
Chen-Mayer HH, Mildner DFR, Lamaze GP, Paul RL, Lindstrom RM (1999) In: Duggan JL, Morgan IL (eds) Application of accelerators in research and industry (AIP Conference proceedings, Vol. 475), Amer Inst Phys, pp 718–721
Chen-Mayer HH, Mackey EA, Paul RL, Mildner DFR (2000) J Radioanal Nucl Chem 244:391
Chen-Mayer HH, Lamaze GP, Mildner DFR, Zeisler R, Gibson WM (2001) Anal Sci 17(Suppl):i629
Chen-Mayer HH, Heward WJ, Paul RL, Klug FJ, Gao Y (2003) J Mater Res 18:2486
Cho H-J, Chung Y-S, Kim Y-J (2005a) Nucl Instrum Meth B229:499
Cho HJ, Chung YS, Kim YJ (2005b) J Radioanal Nucl Chem 264:701
Cho HJ, Chun KJ, Park KW, Chung YS, Kim HR (2007) J Radioanal Nucl Chem 272:403
Choi HD, Firestone RB, Lindstrom RM, Molnár GL, Mughabghab SF, Paviotti-Corcuera R, Révay Z, Trkov A, Zerkin V, Zhou C (2007) Database of prompt gamma rays from slow neutron capture for elemental analysis (STI/PUB/1263). IAEA, Vienna
Chung C (1995) Neutron damage and induced effects on nuclear instruments used for PGAA. In: Alfassi ZB, Chung C (eds) Prompt gamma neutron activation analysis. CRC Press, Boca Raton, pp 37–58
Chung C, Chen YR (1991) Nucl Instrum Meth A301:328
Chung YS, Moon JH, Cho HJ, Kim HR (2007) J Radioanal Nucl Chem 272:391
Comar D, Crouzel C, Chasteland M, Riviere R, Kellershohn C (1969a) The use of neutron capture gamma radiations for the analysis of biological samples. In: DeVoe JR (ed) Modern trends in activation analysis (NBS Spec. Pub. 312). National Bureau of Standards, Washington, pp 114–127
Comar D, Crouzel C, Chasteland M, Riviere R, Kellershohn C (1969b) Nucl Appl 6:344
Copley JRD, Majkrzak CF (1989) Calculations and measurement of the performance of converging neutron guides. In: Majkrzak CF (ed) Thin-film neutron optical devices: mirrors, supermirrors, multilayer monochromators, polarizers, and beam guides (Proc. SPIE 983). Society of Photo-Optical Instrumentation Engineers, Bellingham, pp 93–104
Copley JRD, Stone CA (1989) Nucl Instrum Meth A281:593
Cristache C, Gmeling K, Culicov O, Frontasyeva MV, Toma M, Duliu OG (2009) J Radioanal Nucl Chem 279:7
De Soete D, Gijbels R, Hoste J (1972) Neutron activation analysis. Wiley-Interscience, London
Debertin K, Helmer RG (1988) Gamma- and X-ray spectrometry with semiconductor detectors. North-Holland, Amsterdam
Deconninck G, Demortier G, Bodart F (1981) Atomic Energy Review, Supplement 2, IAEA, Vienna, pp 151–234
Degenaar IH, Blaauw M, Bode P, de Goeij JJM (2004) J Radioanal Nucl Chem 260:311
Dokhale PA, Csikai J, Olah L (2001) Appl Radiat Isot 54:967
Dorsey DJ, Hebner R, Charlton WS (2004) J Compos Mater 38:1505
Dyar MD, Wiedenbeck M, Robertson D, Cross LR, Delaney JS, Ferguson K, Francis CA, Grew ES, Guidotti CV, Hervig RL, Hughes JM, Husler J, Leeman W, McGuire AV, Rhede D, Rothe H,

Paul RL, Richards I, Yates M (2001) Geostandard Newslett 25:441
Ebihara M, Oura Y (2001) Earth Planet Space 53:1039
Ehmann WD, Vance DE (1991) Radiochemistry and nuclear methods of analysis. Wiley, New York
Elekes Z, Belgya T, Molnár GL, Kiss AZ, Csatlós M, Gulyás J, Krasznahorkay A, Máté Z (2003) Nucl Instrum Meth A503:580
Ember PP, Révay Z, Belgya T, Molnar G (2001) Magy Kem Foly 107:438
Ember PP, Belgya T, Molnár GL (2002) Appl Radiat Isot 56:535
Ember PP, Belgya T, Weil JL, Molnár GL (2004) Nucl Instrum Meth B213:406
English GA, Firestone RB, Perry DL, Reijonen J, Ludewigt B, Leung KN, Garabedian G, Molnar G, Révay Z (2004) Nucl Instrum Meth B213:410
English GA, Firestone RB, Perry DL, Reijonen JP, Leung KN, Garabedian GF, Molnár GL, Révay Z (2008) J Radioanal Nucl Chem 277:25
Fazekas B, Molnár GL, Belgya T, Dabolczi L, Simonits A (1997) J Radioanal Nucl Chem 215:271
Fazekas B, Révay Z, Östör J, Belgya T, Molnár G, Simonits A (1999) Nucl Instrum Meth A422:469
Fleming RF (1982) Appl Radiat Isot 33:1263
Freeman JM, Jenkin JG (1966) Nucl Instrum Meth 43:269
Freitas MC, Révay Z, Szentmiklosi L, Dionisio I, Dung HM, Pacheco AMG (2008) J Radioanal Nucl Chem 278:381
Furuta E, Nakahara H, Hatsukawa Y, Matsue H, Sakane H (2008) J Radioanal Nucl Chem 278:553
Gilmore G, Hemingway JD (1995) Practical gamma-ray spectrometry. Wiley, Chichester
Gmeling K, Harangi S, Kasztovszky Z (2005) J Radioanal Nucl Chem 265:201
Gmeling K, Nemeth K, Martin U, Eby N, Varga Z (2007a) J Volcanol Geoth Res 159:70
Gmeling K, Kasztovszky Z, Szentmiklosi L, Revay Z, Harangi S (2007b) J Radioanal Nucl Chem 271:397
Grazman BL, Schweikert EA (1991) J Radioanal Nucl Chem At 152:497
Harrison RK, Landsberger S (2009) Nucl Instrum Meth B267:513
Hatsukawa Y, Oshima M, Hayakawa T, Noh T, Shinohara N (2002) Nucl Instrum Meth A482:328
Heath RL, Helmer RG, Davidson JR, Gehrke RJ (1999) Gamma-ray spectrum catalogue: Ge and Si detector spectra, 4th edn. CD-ROM., 4, CD-ROM. INEEL, Idaho Falls
Helmer RG, Greenwood RC, Gehrke RJ (1971) Nucl Instrum 96:173
Henkelmann R, Born HJ (1973) J Radioanal Chem 16:473
Hilger A, Kardjilov N, Strobl M, Treimar W, Banhart W (2006) Physica B 385–386:1213
Hils T, Boeni P, Stahn J (2004) Focusing parabolic guide for very small samples. Elsevier Science, Physica B-Condensed Matter 350:166–168
Ihnat M (2000) J Radioanal Nucl Chem 245:73
Im HJ, Lee YH, Park YJ, Song BC, Cho J, Kim WH (2007) Nucl Instrum Meth A574:272
Im HJ, Song K (2009a) Appl Spectrosc Rev 44:317
Im HJ, Song BC, Park YJ, Song K (2009b) Classification of materials for explosives from prompt gamma spectra by using principal component analysis. Pergamon-Elsevier Science, Appl Rad Isot 67:1458–1462
Isenhour TL, Morrison GH (1966a) Anal Chem 38:162
Isenhour TL, Morrison GH (1966b) Anal Chem 38:167
Johansen GA, Jackson P (2004) Radioisotope gauges for industrial process measurements. Wiley, Chichester
Jones CY, Wu J, Li LP, Haile SM (2005) J Appl Phys 97:114908
Jordanov VT, Knoll GF, Huber AC, Pantazis JA (1994) Nucl Instrum Meth A353:261
Jurney ET, Starner JW, Lynn JE, Raman S (1997) Phys Rev C 56:118
Kasviki K, Stamatelatos IE, Kalef-Ezra J (2007a) Evaluation of spatial sensitivity of a prompt gamma neutron activation analysis facility for the in vivo determination of nitrogen in small animals. Springer, Berlin, pp 225–231
Kasviki K, Stamatelatos IE, Yannakopoulou E, Papadopoulou P, Kalef-Ezra J (2007b) Nucl Instrum Meth B263:3
Kasztovszky Z, Révay Z, Belgya T, Fazekas B, Östör J, Molnár GL, Molnar G, Borossay J (1999) J Anal Atom Spectrom 14:593
Kasztovszky Z, Révay Z, Belgya T, Molnár GL (2000) J Radioanal Nucl Chem 244:379
Kasztovszky Z, Révay Z, Molnar G, Wootsch A, Paal Z (2002) Catal Comm 3:553
Kasztovszky Z, de Antczak MM, Antczak A, Milian B, Bermudez J, Sajo-Bohus L (2004) Nukleonika 49:107
Kasztovszky Z, Panczyk E, Fedorowicz W, Révay Z, Sartowska B (2005) J Radioanal Nucl Chem 265:193
Kasztovszky Z, Visser D, Kockelmann W, Pantos E, Brown A, Blaauw M, Hallebeek P, Veerkamp J, Krook W, Stuchfield HM (2007) Nuovo Cimento 30:67
Kasztovszky Z, Biro KT, Marko A, Dobosi V (2008a) Archaeometry 50:12
Kasztovszky Z, Biro KT, Marko A, Dobosi V (2008b) J Radioanal Nucl Chem 278:293
Kasztovszky Z, Kis Z, Belgya T, Kockelmann W, Imberti S, Festa G, Filabozzi A, Andreani C, Kirfel A, Biro KT, Duzs K, Hajnal Z, Kudejova P, Tardocchi M (2008c) J Radioanal Nucl Chem 278:661
Kasztovszky Z, Kockelmann WA, Cippo EP, Gorini G, Tardocchi M (2008d) Nuovo Cimento 31:143
Kis Z, Fazekas B, Östör J, Révay Z, Belgya T, Molnár GL, Koltay L (1998) Nucl Instrum Methods A418:374

Knoll GF (2000) Radiation detection and measurement. Wiley, New York
Kobayashi T, Kanda K (1983) Nucl Instrum Meth 204:525
Krusche B, Lieb KP, Daniel H, von Egidy T, Barreau G, Börner HG, Brissot R, Hofmeyr C, Rascher R (1982) Nucl Phys A386:245
Kudejova P, Materna T, Jolie J, Turler A, Wilk P, Baechler S, Kasztovszky Z, Révay Z, Belgya T (2005) J Radioanal Nucl Chem 265:221
Kudejova P, Meierhofer G, Zeitelhack K, Jolie J, Schulze R, Turler A, Materna T (2008) J Radioanal Nucl Chem 278:691
Kudejova P, Canella L, Schulze R, Jolie J, Turler A (2009) New PGAI-NT and PGAA at FRM II for geological samples: test measurements on allende meteorite. Pergamon-Elsevier Science, Geochim Cosmichim Acta 73(Suppl):A701–A701
Kvardakov VV, Chen-Mayer HH, Mildner DFR, Somenkov VA (1998) J Appl Phys 83:3876
Lea DE (1934) Nature 133:24
Lehmann EH, Vontobel P, Frei G (2007) Nuovo Cimento C 30:93
Leo WR (1987) Techniques for nuclear and particle physics experiments. Springer, Berlin
Lim CS, Sowerby BD (2005) J Radioanal Nucl Chem 264:4
Lindstrom DJ (1990) Nucl Instrum Meth A299:584
Lindstrom RM (1998) Fresenius J Anal Chem 360:322
Lindstrom RM (2003) J Radioanal Nucl Chem 257:557
Lindstrom RM, Lindstrom DJ, Slaback LA, Langland JK (1990) Nucl Instrum Meth A299:425
Lindstrom RM, Zeisler R, Vincent DH, Greenberg RR, Stone CA, Mackey EA, Anderson DL, Clark DD (1993) J Radioanal Nucl Chem At 167:121
Lone MA, Santry DC, Inglis WM (1980) Nucl Instrum Meth 174:521
Lone MA, Leavitt RA, Harrison DA (1981) At Data Nucl Data Tables 26:511
Mackey EA, Copley JRD (1993) J Radioanal Nucl Chem 167:127
Mackey EA, Spatz RO (2009) J Radioanal Nucl Chem 281:91
Mackey EA, Gordon GE, Lindstrom RM, Anderson DL (1991) Anal Chem 63:288
Mackey EA, Anderson DL, Liposky PJ, Lindstrom RM, Chen-Mayer H, Lamaze GP (2004) Nucl Instrum Meth B226:426
Mackey EA, Cronise MP, Fales CN, Greenberg RR, Leigh SD, Long SE, Marlow AF, Murphy KE, Oflaz R, Sieber JR, Rearick MS, Wood LJ, Yu LL, Wilson SA, Briggs PH, Brown ZA, Budahn J, Kane PF, Hall WL (2007) Anal Bioanal Chem 387:2401
Maier-Leibnitz H (1969) Neutron conducting tubes. In: Ryde N (ed) Neutron-capture gamma-ray spectroscopy (STI/PUB/235). IAEA, Vienna, pp 93–103
Manescu A, Fiori F, Giuliani A, Kardjilov N, Kasztovszky Z, Rustichelli F, Straumal B (2008) J Phys-Condens Mat 20:104250
Marschall HR, Kasztovszky Z, Gmeling K, Altherr R (2005) J Radioanal Nucl Chem 265:339
Marschall HR, Altherr R, Gmeling K, Kasztovszky Z (2009) Mineral Petrol 95:291
Martinho E, Gonçalves IF, Salgado J (2003) Appl Radiat Isot 58:371
Matsue H, Yonezawa C (2001) J Radioanal Nucl Chem 249:11
Matsumoto T, Aizawa O, Nozaki T, Sato T (1984) Atomkernenergie 44:566
Mildner DFR, Chen-Mayer HH (1999) Nucl Instrum Meth At 422: 21
Mildner DFR, Chen-Mayer HH, Gibson WM (2002) J Appl Phys 92:6911
Miri-Hakimabad H, Panjeh H, Vejdani-Noghreiyan A (2008) Nucl Sci Tech 19:109
Miura T, Matsue H, Kuroiwa T, Chiba K (2008) J Radioanal Nucl Chem 278:653
Miyoshi M, Shimono M, Hasenaka T, Sano T, Fukuoka T (2008) J Radioanal Nucl Chem 278:343
Molnár GL (2004) Handbook of prompt gamma activation analysis with neutron beams. Kluwer, Dordrecht
Molnár G, Belgya T, Dabolczi L, Fazekas B, Révay Z, Veres Á, Bikit I, Kiss Z, Östör J (1997) J Radioanal Nucl Chem 215:111
Molnár GL, Révay Z, Paul RL, Lindstrom RM (1998) J Radioanal Nucl Chem 234:21
Molnár GL, Révay Z, Belgya T, Firestone RB (2000) Appl Radiat Isot 53:527
Molnár GL, Belgya T, Révay Z, Qaim SM (2002a) Radiochim Acta 90:479
Molnár GL, Révay Z, Belgya T (2002b) Nucl Instrum Meth 489:140
Molnár GL, Révay Z, Belgya T (2004) Nucl Instrum Meth B213:389
Moody JR, Greenberg RR, Pratt KW, Rains TC (1988) Anal Chem 60:1203A
Morgan WD (2000) In: Yasumura S, Wang J, Pierson RN (eds) Of mermaids and mountains – three decades of prompt activation in vivo., pp 128–133
Naqvi AA, Nagadi MM (2004) J Radioanal Nucl Chem 260:641
Nunez-Lagos R, Virto A (1996) Appl Radiat Isot 47:1011
O'Meara JM, Blackburn BW, Chichester DL, Gierga DP, Yanch JC (2001) Appl Radiat Isot 55:767
Orphan VJ, Rasmussen NC (1967) Nucl Instrum Meth 48:282
Orphan VJ, Rasmussen NC, Harper TL (1970) In: Report DASA 2570 (GA 10278), Gulf General Atomic, San Diego, 685
Oura Y, Nakahara H, Sueki K, Sato W, Saito A, Tomizawa T, Nishikawa T (1999) Czech J Phys Suppl 49:311

Oura Y, Iguchi H, Nagahata T, Nakamatsu H, Otoshi T, Ebihara M (2007) J Radioanal Nucl Chem 272:381
Owens A (1989) Nucl Instrum Meth A274:297
Owens A, Gehrels N, Pascarelle SM, Teegarden BJ (1991) IEEE Trans Nucl Sci 38:221
Paglia G, Buckley CE, Udovic TJ, Rohl AL, Jones F, Maitland CF, Connolly J (2004) Chem Mater 16:1914
Pallone AK, Demaree JD (2009) Nucl Instrum Meth B267:2927
Park CS, Sun GM, Byun SH, Choi HD (2005) J Radioanal Nucl Chem 265:283
Park CS, Sun GM, Choi HD (2006) Nucl Instrum Meth B245:367
Park YJ, Song BC, Chowdhury MI, Jee KY (2004) J Radioanal Nucl Chem 260:585
Park YJ, Song BC, Im HJ, Kim JY (2009) Nucl Instrum Meth A606:243
Paul R, Mackey EA, Zeisler R, Spatz RO, Tomlin BE (2009) J Radioanal Nucl Chem 282:945
Paul RL (1997) Analyst 122:R35
Paul RL (2001) Analyst 126:217
Paul RL (2005) Analyst 130:99
Paul RL, Lindstrom RM (2000) J Radioanal Nucl Chem 243:181
Perego RC, Blaauw M (2005) J Appl Phys 97:123533
Perry DL, Firestone RB, Molnár GL, Révay Z, Kasztovszky Z, Gatti RC, Wilde P (2002) J Anal Atom Spectrom 17:32
Perry DL, English GA, Firestone RB, Molnár GL, Révay Z (2005) J Radioanal Nucl Chem 265:229
Perry DL, English GA, Firestone RB, Leung KN, Garabedian G, Molnár GL, Révay Z (2008) J Radioanal Nucl Chem 276:273
Phillips GW, Marlow KW (1976a) Nucl Instrum Meth 72:125
Phillips GW, Marlow KW (1976b) Nucl Instrum Meth 137:525
Postma H, Schillebeeckx P (2005) J Radioanal Nucl Chem 265:297
Postma H, Perego RC, Schillebeeckx P, Siegler P, Borella A (2007) Neutron resonance capture analysis and applications. Springer, Berlin, pp 95–99
Rasmussen NC, Hukai Y, Inouye T, Orphan VJ (1969) Thermal neutron capture gamma-ray spectra of the elements, Report AFCRL-69-0071. Massachusetts Institute of Technology, Boston
Reijonen J, Leung KN, Firestone RB, English JA, Perry DL, Smith A, Gicquel F, Sun M, Koivunoro H, Lou TP, Bandong B, Garabedian G, Révay Z, Szentmiklosi L, Molnar G (2004) Nucl Instrum Meth At 522:598
Révay Z (2005) J Radioanal Nucl Chem 264:283
Révay Z (2006) Nucl Instrum Meth A564:688
Révay Z (2008) J Radioanal Nucl Chem 276:825
Révay Z (2009) Anal Chem 81:6851
Révay Z, Molnár GL, Belgya T, Kasztovszky Z, Firestone RB (2000) J Radioanal Nucl Chem 244:383
Révay Z, Molnár GL, Belgya T, Kasztovszky Z, Firestone RB (2001a) J Radioanal Nucl Chem 248:395
Révay Z, Belgya T, Ember PP, Molnár GL (2001b) J Radioanal Nucl Chem 248:401
Révay Z, Molnár GL, Belgya T, Kasztovszky Z (2003) J Radioanal Nucl Chem 257:561
Révay Z, Belgya T, Kasztovszky Z, Weil JL, Molnár GL (2004) Nucl Instrum Meth B 213:385
Révay Z, Belgya T, Szentmiklósi L, Molnár GL (2005) J Radioanal Nucl Chem 264:277
Révay Z, Belgya T, Molnár GL, Rausch H, Braun T (2006) Chem Phys Lett 423:450
Révay Z, Harrison RK, Alvarez E, Biegalski SR, Landsberger S (2007) Nucl Instrum Meth A577:611
Révay Z, Belgya T, Szentmiklosi L, Kis Z (2008a) J Radioanal Nucl Chem 278:643
Révay Z, Belgya T, Szentmiklosi L, Kis Z, Wootsch A, Teschner D, Swoboda M, Schlogl R, Borsodi J, Zepernick R (2008b) Anal Chem 80:6066
Rios-Martinez C, Unlu K, Wehring BW (1998) J Radioanal Nucl Chem 234:119
Robinson JA, Hartman MR, Reese SR (2009) J Radioanal Nucl Chem. doi:10.1007/s10967-009-0358-2
Rogante M, De Marinis G, Kasztovszky Z, Milazzo F (2007) Nuovo Cimento C 30:113
Rossbach M (1991) Anal Chem 63:2156
Sah RN, Brown PH (1997) Microchem J 56:285
Sajo-Bohus LS, de Antczak MMM, Greaves ED, Antczak A, Bermudez J, Kasztovszky Z, Poirier T, Simonits A (2005) J Radioanal Nucl Chem 265:247
Sajo-Bohus L, Mackowiak deAntczak, M. M., Kastovszky Z, Greaves ED, Antczak A, Simonits A, Palacios D, Millan B (2006) J Phys Conference Series 41:8
Sakai Y, Kubo MK, Matsue H, Yonezawa C (2005) J Radioanal Nucl Chem 265:287
Sandor Z, Tolgyesi S, Gresits I, Kasztovszky Z (2002) J Radioanal Nucl Chem 254:283
Segawa M, Matsue H, Sekiya Y, Yamada S, Shinohara T, Oku T, Sasao H, Suzuki J, Shimizu HM (2008) J Radioanal Nucl Chem 278:647
Sieber JR, Mackey EA, Marlow AF, Paul R, Martin R (2007) Powder Diffr 22:146
Stone CA, Blackburn DH, Kauffman DA, Cranmer DC, Olmez I (1994) Nucl Instrum Meth A349:515
Sueki K, Kobayashi K, Sato W, Nakahara H, Tomizawa T (1996) Anal Chem 68:2203
Sueki K, Oura Y, Sato W, Nakahara H, Tomizawa T (1998) J Radioanal Nucl Chem 234:27
Sun G, Park C, Choi H (2008) J Radioanal Nucl Chem 278:637
Sun GM, Byun SH, Choi HD (2003) J Radioanal Nucl Chem 256:541
Sun GM, Park CS, Choi HD (2005) J Radioanal Nucl Chem 264:603
Swider JR, Walters WB (2004) Nucl Instrum Meth B 226:659

Swider JR, Mustillo DM, Conticchio LF, Walters WB, Paul RL, Lindstrom RM (1994) In: Kern J (ed) Proceedings of the 8th international symposium on capture gamma-ray spectroscopy and related topic, World Scientific, Singapore, pp 335–337

Szakmany G, Kasztovszky Z (2004) Eur J Mineralog 16:285

Szentmiklosi L, Belgya T, Révay Z (2005) J Radioanal Nucl Chem 264:229

Szentmiklosi L, Révay Z, Belgya T (2006a) Nucl Instrum Meth At 564:655

Szentmiklosi L, Révay Z, Chobola R, Mell P, Szakacs S, Kasa I (2006b) J Radioanal Nucl Chem 267:415

Szentmiklosi L, Gmeling K, Révay Z (2007a) J Radioanal Nucl Chem 271:447

Szentmiklosi L, Révay Z, Belgya T (2007b) Nucl Instrum Meth B 263:90

Szentmiklosi L, Révay Z, Belgya T, Simonits A, Kis Z (2008) J Radioanal Nucl Chem 278:657

Teschner D, Borsodi J, Wootsch A, Révay Z, Havecker M, Knop-Gericke A, Jackson SD, Schlogl R (2008) Science 320:86

Toh Y, Oshima M, Kimura A, Koizumi M, Furutaka K, Hatsukawa Y, Goto J (2008) J Radioanal Nucl Chem 278:685

Tompa K, Banki P, Bokor M, Lasanda G, Vasaros L (2003) J Alloy Compd 350:52

Turhan S, Yucel H, Demirbas A (2004) J Radioanal Nucl Chem 262:661

Unlu K, Rios-Martinez C (2005) J Radioanal Nucl Chem 265:329

van den Berg AWC, Pescarmona PP, Schoonman J, Jansen JC (2007) Chem Eur J 13:3590

Westcott CH (1955) J Nucl Energy 2:59

Wehring BW, Unlu K, Rios-Martinez C (1997) Appl Rad Isotopes 48:1343

Wilhelm M, Eberth J, Pascovici G, Radermacher E, Thomas HG, vonBrentano P, Prade H, Lieder RM (1996) Nucl Instrum Meth A381:462

Yamauchi S, Sakai Y, Watanabe Y, Kubo MK, Matsue H (2005) In: Proceedings of the 55th annual meeting of the Japan-Wood-Research-Society, Kyoto, Japan, March. Springer, Tokyo, pp 279–281

Yamazaki S, Oura Y, Ebihara M (2007) J Radioanal Nucl Chem 272:353

Yonezawa C, Wood AKH, Magara M, Sawahata S, Hoshi M, Ito Y, Tachikawa E (1993) Prompt gamma-ray analysis using JRR-3M cold and thermal neutron guide beams. In: Proceedings of the 5th international symposium advanced nuclear energy research (JAERI-M 93-228), Mito, Japan, vol 2. JAERI, Tokai, pp 854–861

Yonezawa C (1999) Biol Trace Elem Res 71–2:407

Yonezawa C (2002) Bunseki Kagaku 51:61

Young SK, Trevino SF, Tan NCB, Paul RL (2003) J Polym Sci B41:1485

Zeisler R, Lamaze GP, Chen-Mayer HH (2001) J Radioanal Nucl Chem 248:35

Zeisler R, James WD, Mackey EA, Spatz RO, Greenberg RR (2008) J Radioanal Nucl Chem 278:783

Zhang L, Ni B, Tian W, Huang D, Zhang G, Liu C, Wang P, Liu L, Li D (2005) Atom Energy Sci Tech 39:282

Zhao L, Robinson L (2009) J Radioanal Nucl Chem 282:151

Zhao L, Robinson L, Mackey EA, Paul RL, Greenberg RR (2008) J Radioanal Nucl Chem 277:275